

1 **Exploring the high load potential of diesel-methanol dual-fuel**
2 **operation with Miller cycle, EGR, and intake air cooling on a**
3 **heavy-duty diesel engine**

4
5 **Wei Guan^{1,2}, Xinyan Wang¹, Hua Zhao¹, Haifeng Liu³**

6 ¹Brunel University London, London, United Kingdom

7 ²Guangxi Yuchai Machinery Company, Yulin, China

8 ³Tianjin University, Tianjin, China

9

10 **Abstract**

11 Legislations concerning emissions from heavy-duty (HD) diesel engines are becoming
12 increasingly stringent. This requires conventional diesel combustion (CDC) to be compliant
13 using costly and sophisticated aftertreatment systems. Preferably, Diesel-methanol dual-fuel
14 (DMDF) is one of the suitable alternative combustion modes as it can potentially reduce the
15 formation of NO_x and soot emissions which characterised the diesel mixing-controlled
16 combustion. This is primarily due to the high latent heat of vaporisation and oxygen content of
17 the methanol fuel. At high engine loads, however, the potential of DMDF operation is
18 constrained by the excessive combustion pressure rise rate (PRR) and peak in-cylinder pressure,
19 which limits both the engine efficiency and the percentage of methanol that can be used. For
20 the first time, experimental studies were conducted to explore advanced combustion control
21 strategies such as Miller cycle, exhaust gas recirculation (EGR), and intake air cooling for
22 improving upon high-load DMDF combustion. Experiments were carried out at 1200 rpm and
23 18 bar indicated mean effective pressure (IMEP) on a single cylinder HD diesel engine, which

24 equipped with a high pressure common rail diesel injection, a methanol port fuel injection, and
25 a variable valve actuation system on the intake camshaft.

26 Results showed that the methanol energy fraction (MF) of a conventional DMDF operation
27 with a baseline intake valve closing (IVC) timing was limited to 28%. This was due to the high
28 combustion temperature at a high load which advanced the ignition timing of the premixed
29 charge, resulting in high levels of PRR. The application of lower effective compression ratio
30 (ECR) and intake air temperature (T_{int}) effectively decreased the compression temperature,
31 which successfully delayed the ignition timing of the premixed charge. This allowed for a more
32 advanced diesel injection timing to achieve improvement in the thermal efficiency and
33 potentially enabled a higher methanol substitution ratio. Although the introduction of EGR
34 demonstrated very slight impact on the ignition timing of the premixed charge, a higher net
35 indicated efficiency was observed due to a relatively lower local combustion temperature
36 which reduced heat transfer loss. Moreover, the optimised DMDF operation allowed a higher
37 MF of 40% to be used at an ECR of 14.3 and T_{int} of 305 K and achieved the highest net indicated
38 efficiency of 47.4%, improving by 3.7% and 2.6% respectively when compared to the
39 optimised CDC (45.7%) and conventional DMDF (46.2%). This improvement was
40 accompanied with a reduction of 37% in NO_x emissions and little impact on soot emissions in
41 comparison with the CDC.

42 **Keywords**

43 Heavy-duty diesel engine, methanol, dual-fuel, Miller cycle, EGR, intake air cooling

44 **1. Introduction**

45 According to the most comprehensive assessment of climate change undertaken by the
46 Intergovernmental Panel on Climate Change, the global warming is strongly related to the

47 burning of fossil fuels which add a substantial amount of greenhouse gases (GHG) such as CO₂
48 into the atmosphere [1]. Among different sources, CO₂ emissions produced by transportation
49 are the largest sector [2]. In particular, the commercial sector, namely HD trucks, with 4% of
50 the total number of on-road vehicles, accounts for 18% of the fuel consumption and CO₂
51 emissions within the transportation sector [3]. In addition to GHG emissions, pollutants such
52 as NO_x and soot are of increasing concern as they have significantly harmful impact on human
53 health and environment. These issues are driving the development of powertrain technology
54 and the exploration of alternative advanced combustion modes.

55 Conventional diesel combustion (CDC) is suffered from the typical NO_x-soot trade-off. Their
56 formation is due to the fact that the non-premixed diffusion-controlled combustion is
57 characterised by a wide range of local in-cylinder gas temperatures and equivalence ratios [4].
58 To comply with strict emissions regulations, costly and sophisticated aftertreatment systems
59 are essential [5].

60 In last few decades, numerous research has focused on low temperature combustion (LTC)
61 modes, which includes Homogeneous Charge Compression Ignition (HCCI) [6], Premixed
62 Charge Compression Ignition (PCCI) [7], Partially Premixed Charge Compression Ignition
63 (PPCI) [8], Modulated Kinetics (MK) [9], and Uniform Bulky Combustion System (UNIBUS)
64 [10]. These allow a higher degree of combustion phasing control at low and medium loads and
65 have shown their potential to achieve simultaneous low levels of NO_x and soot emissions.
66 However, these combustion modes suffer from high unburned HC and CO emissions, lack of
67 combustion phasing control, and limited load range operation.

68 Interest in renewable alternatives for heavy-duty applications to partially replace fossil fuel has
69 achieved fast grow in recent years. Dual-fuel (DF) combustion, such as Reactivity Controlled
70 Compression Ignition (RCCI), has been researched as a method to effectively use alternative

71 fuels in conventional diesel engines and developed to overcome the previously mentioned
72 issues [11–13]. The method separates the fuel delivery, port fuel injection of the low reactivity
73 fuel such as gasoline, natural gas, methanol, and ethanol while directly injecting the high
74 reactivity fuel (e.g. diesel) to serve as the ignition source. Among the low reactivity fuels,
75 methanol is one of the most promising alternative fuels for internal combustion engines as it
76 can be produced from renewable sources. Methanol can be produced from various resources
77 including biomass, natural gas, hydrogen, coal, and coke-oven gas, which thus can be a superior
78 fuel for long-term and widespread replacement of conventional fossil fuels. Methanol is also a
79 high oxygen content fuel with high latent heat of vaporisation, having the potential to reduce
80 NO_x and smoke emissions [14–16].

81 This concept has been shown to enable reactivity stratification controlled by the direct-injection
82 of diesel, allowing for a wide range of operation with acceptable pressure rise rate [17,18]. A
83 number of studies revealed that an optimised DF combustion can achieve lower levels of NO_x
84 and soot, and a better thermal efficiency in comparison with the CDC operation [19–21].
85 However, high-load DF operations suffer from high levels of PRR and peak in-cylinder
86 pressure limitations due to the autoignition and fast combustion of the premixed fuel, which
87 associated with the high combustion temperature at a high load [14,22].

88 The use of EGR has been proven as an effective method to extend the high-load DF operation.
89 This is associated with a reduction in the combustion temperature due to the increased specific
90 heat capacity and dilution level of the in-cylinder charge [23,24], which delays the ignition
91 time of the premixed fuel and thus allows for a high-load DF operation with low levels of PRR
92 and NO_x emissions [25–28]. Additionally, the application of a lower compression ratio has
93 attracted more attention for the suppression of in-cylinder gas pressure and temperature at high
94 load operation [29–31]. Particularly, the use of Miller cycle to achieve variable compression
95 ratio via early intake valve closing (EIVC) or late intake valve closing timings (LIVC) has been

96 mostly focused on [32–34]. This is attributed to the effectiveness of Miller cycle in reducing
97 the in-cylinder gas temperature and pressure during compression strokes, allowing for a more
98 flexible combustion control of both injected fuels over the engine cycles. On the other hand,
99 the delayed intake valve closure decreases the in-cylinder charge density and oxygen
100 availability. This can increase the average in-cylinder gas temperature due to lower total heat
101 capacity [35] and adversely affect combustion process due to lower air-fuel ratio [36],
102 potentially decreasing the engine efficiency [37].

103 Moreover, the intake air cooling is another effective combustion control strategy used for
104 overcoming the limitation of high load DF combustion. Pedrozo et al. [30] experimentally
105 investigated ethanol-diesel dual-fuel operating with Miller cycle and intake air cooling at high
106 load. They found that a reduction in the intake air temperature can suppress the early ignition
107 of ethanol, allowing for a substantial improvement in the maximum ethanol energy fraction,
108 net indicated efficiency, and NO_x emissions. Wang et al. [38] and Varde [16] also revealed that
109 decreasing intake air temperature can effectively minimise the maximum in-cylinder gas
110 pressure (P_{\max}) and PRR by delaying the ignition timing of the premixed fuel derived from the
111 port-injection.

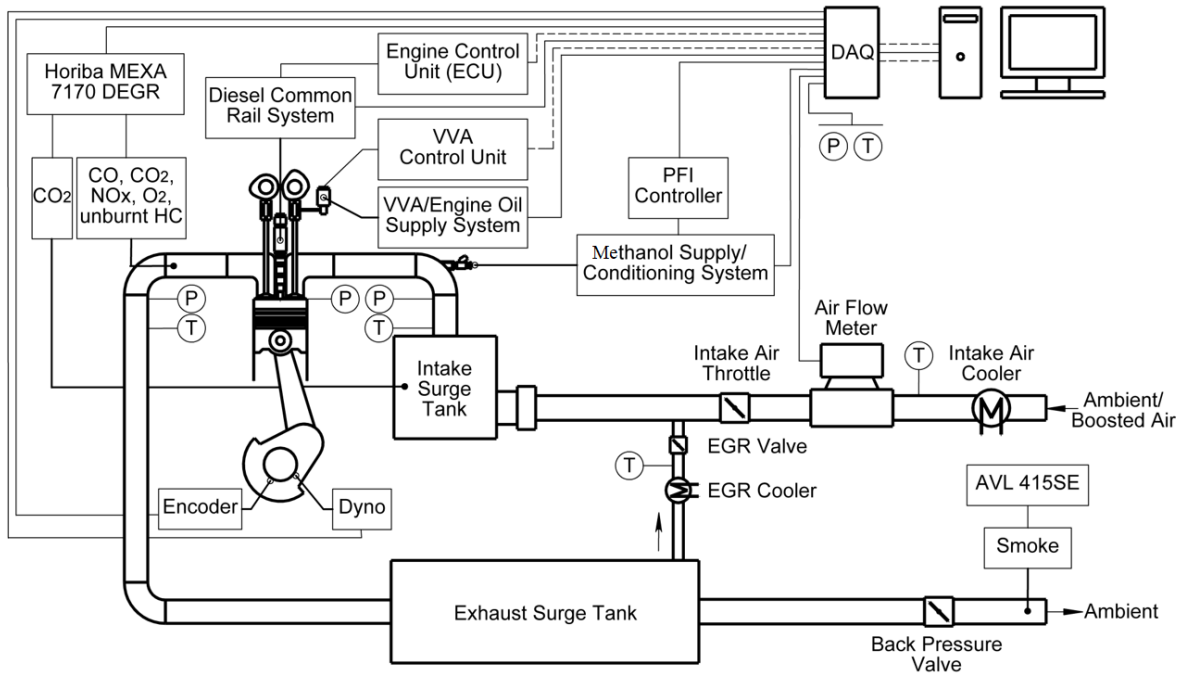
112 Considering the majority of previous works were performed individually to investigate the
113 effects of EGR, intake cooling, and Miller cycle on the DMDF operation, a systematic
114 experimental study was carried out on a single cylinder heavy-duty diesel engine to
115 comprehensively analysed their potential for increasing the maximum net indicated efficiency.
116 Advanced combustion control strategies were explored to improve the high load DMDF
117 operation with high efficiency and low levels of NO_x and soot emissions. To the best of our
118 knowledge, the current work is the first attempt to experimentally investigate and compare the
119 potential of high load methanol-diesel dual-fuel operation with EGR, Miller cycle, and intake
120 air cooling.

121 The experiments were performed at 1200 rpm and 18 bar IMEP with varying diesel injection
122 timings to up to the PRR and in-cylinder pressure limitations. Specifically, the low reactivity
123 fuel via port fuel injection was methanol while the diesel fuel was directly injected into the
124 cylinder as an ignition source. The effects of methanol energy fraction, EGR, Miller cycle, and
125 intake air cooling were evaluated. The potential of DMDF operation with Miller cycle and
126 intake air cooling was analysed. Finally, the optimised advanced DMDF results were compared
127 against the optimised CDC and conventional DMDF operations.

128 **2. Experimental setup**

129 **2.1 Engine specifications and experimental facilities**

130 Figure 1 shows the schematic diagram of the single cylinder heavy-duty diesel engine. A
131 Froude Hofmann AG150 eddy current dynamometer was coupled to absorb the engine power
132 output. Table 1 outlines the base hardware specifications of the test engine. The combustion
133 system was designed based on a production Yuchai YC6K 6-cylinder diesel engine, which
134 consisted of a 4-valve swirl-oriented cylinder head and a stepped-lip piston bowl design with
135 a geometric compression ratio of 16.8. The bottom end/short block was AVL-designed with
136 two counter-rotating balance shafts.



137

138

Figure 1. Layout of the engine experimental setup.

139

Table 1. Specifications of the test engine.

Displaced Volume	2026 cm ³
Stroke	155 mm
Bore	129 mm
Connecting Rod Length	256 mm
Geometric Compression Ratio	16.8
Number of Valves	4
Piston Type	Stepped-lip bowl
Diesel Injection System	Bosch common rail
Nozzle design	8 holes, 0.176 mm hole diameter, included spray angle of 150°
Maximum fuel injection pressure	2200 bar
Maximum in-cylinder pressure	180 bar

140

141 The compressed air was supplied by an AVL 515 sliding vanes supercharger with closed loop

142 control. Two surge tanks were installed to damp out the strong pressure fluctuations in intake

143 and exhaust manifolds. The intake manifold pressure was finely controlled by a throttle valve
 144 located upstream of the intake surge tank. An Endress+Hauser Proline t-mass 65F thermal mass
 145 flow meter was used to measure the fresh air mass flow rate. An electronically controlled
 146 butterfly valve located downstream of the exhaust surge tank was used to independently control
 147 the exhaust back pressure. High-pressure loop cooled external EGR was introduced to the
 148 engine intake manifold located between the intake surge tank and throttle by using a pulse
 149 width modulation-controlled EGR valve and the pressure differential between the intake and
 150 exhaust manifolds. Coolant and oil pumps were driven by separate electric motors. Water
 151 cooled heat exchangers were used to control the temperatures of the boosted intake air and
 152 external EGR as well as engine coolant and lubricating oil. The coolant and oil temperatures
 153 were kept within 356 ± 2 K. The oil pressure was maintained within 4.0 ± 0.1 bar throughout
 154 the experiments. The specifications of the measurement equipment can be found in Appendix
 155 A.

156 **2.2 Fuel properties and fuelling system**

157 Table 2 shows the diesel and methanol fuel properties. During the dual-fuel operation,
 158 methanol was injected through a port fuel injector. The desired methanol energy fraction was
 159 achieved via adjusting the PFI pulse width controlled by an injector driver. The methanol mass
 160 flow rate ($\dot{m}_{methanol}$) was obtained from an injector calibration curve determined with a semi-
 161 microbalance with an accuracy of ± 0.1 mg. Methanol injection pressure was continuously
 162 monitored to maintain a constant relative pressure of 3.0 bar across the injector. The methanol
 163 temperature was kept between 292 and 298 K through a heat exchanger.

164 Table 2. Fuel properties of diesel and methanol.

Properties	Red diesel	Methanol
Density at 293 K (ρ)	0.827 kg/dm ³	0.791 – 0.794 g/mL 20 °C

Cetane number	> 45	4
Research octane number (RON)	n/a	109
Water content	< 0.20 g/kg	NMT 0.1% wt (1000 ppm)
Heat of vaporisation	270 kJ/kg	1.11 MJ/kg
Carbon mass content	86.6%	37.5 (wt.%)
Hydrogen mass	13.2%	12.5%
Oxygen mass content	0.2%	50%
Molecular formula	$CH_{1.825}O_{0.0014}$	CH_3OH
Lower heating value (LHV)	42.9×10^6 J/kg	20.27×10^6 J/kg

165

166 The diesel fuel injection parameters such as injection pressure, start of injection (SOI), and the
167 number of injections were controlled by a dedicated electronic control unit (ECU). During the
168 experiments, the diesel fuel rate (\dot{m}_{diesel}) was injected into the engine by a high-pressure
169 solenoid injector through a high pressure pump and a common rail with a maximum fuel
170 pressure of 2200 bar. The fuel consumption was determined by measuring the total fuel
171 supplied to and from the high pressure pump and diesel injector via two Coriolis flow meters.

172 The methanol energy fraction (MF) was defined as the ratio of the energy content of the
173 methanol to the total fuel energy by

$$174 \quad MF\% = \frac{\dot{m}_{methanol} LHV_{methanol}}{\dot{m}_{methanol} LHV_{methanol} + \dot{m}_{diesel} LHV_{diesel}} \quad (1)$$

175 The actual lower heating value of the in-cylinder fuel mixture (LHV_{DF}) was calculated as

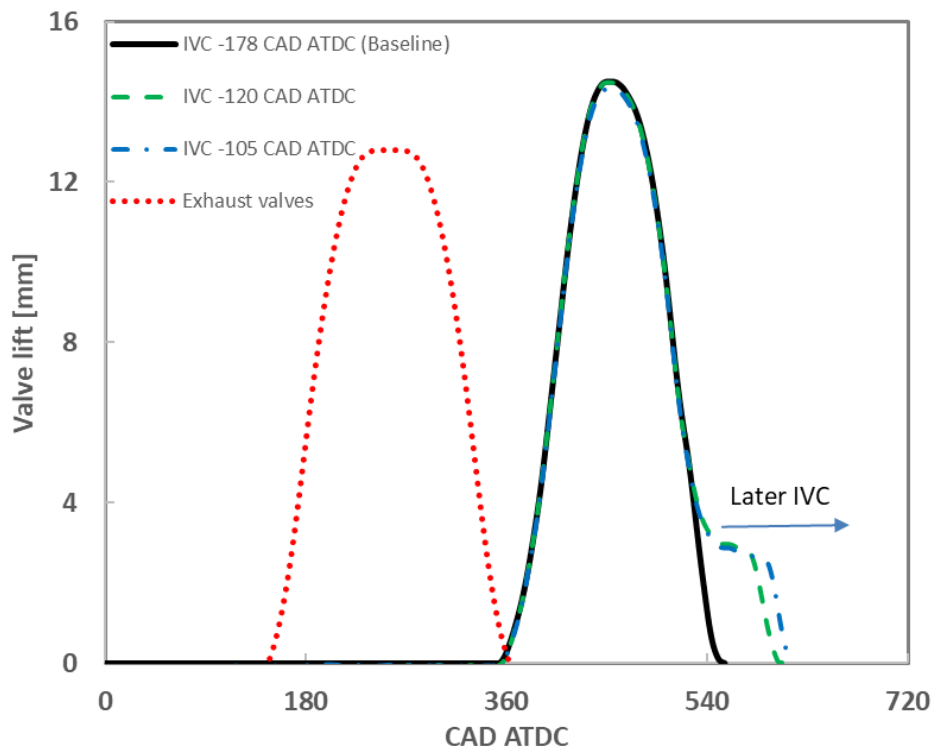
176
$$LHV_{DF} = \frac{(\dot{m}_{methanol}LHV_{methanol}) + (\dot{m}_{diesel}LHV_{diesel})}{\dot{m}_{methanol} + \dot{m}_{diesel}} \quad (2)$$

177 **2.3 Variable valve actuation system**

178 The engine was equipped with a prototype hydraulic lost-motion VVA system, which
179 incorporated a hydraulic collapsing tappet on the intake valve side of the rocker arm. The VVA
180 system allowed for the adjustment of the IVC timing and thus enabled Miller cycle operation.
181 The intake valve opening (IVO) and closing (IVC) of the baseline case were set at 367 and -
182 178 crank angle degrees (CAD) after top dead centre (ATDC), respectively. All valve events
183 were considered at 1 mm valve lift and the maximum intake valve lift event was set to 14 mm.
184 Figure 2 shows the intake and exhaust valve profiles for the baseline and Miller cycle
185 operations. The effective compression ratio, ECR, was calculated as

186
$$ECR = \frac{V_{ivc_eff}}{V_{tdc}} \quad (3)$$

187 where V_{tdc} is the cylinder volume at top dead centre (TDC) position, and V_{ivc_eff} is the
188 effective cylinder volume where the in-cylinder compressed air pressure is extrapolated to be
189 identical to the intake manifold pressure [39,40].



190

191

Figure 2. Fixed exhaust and variable intake valve lift profiles.

192 2.4 Exhaust emissions measurement

193 A Horiba MEXA-7170 DEGR emission analyser was used to measure the exhaust gases such

194 as NO_x , HC, CO, and CO_2 in the exhaust pipe before the exhaust back pressure valve. In this

195 analyser system, gases including CO and CO_2 were measured through a non-dispersive infrared

196 absorption (NDIR) analyser, HC was measured by a flame ionization detector (FID), and NO_x

197 was measured by a chemiluminescence detector (CLD). Specifically, the FID response was

198 corrected by a similar method developed by Kar and Cheng [41] to account for the oxygenated

199 organic species resultant from methanol combustion. To allow for the measurement at elevated

200 back pressure, a high pressure sampling module was used between the exhaust sampling point

201 and the emission analyser. A heated line was deployed to maintain the exhaust gas sample

202 temperature of approximately 192°C to avoid condensation. The smoke number was measured

203 downstream of the exhaust back pressure valve using an AVL 415SE Smoke Meter. The

204 measurement was taken in filter smoke number (FSN) basis and thereafter was converted to

205 mg/m³ [42]. All the exhaust gas components were converted to net indicated specific gas
206 emissions (in g/kWh) according to [43]. In this study, the EGR rate was defined as the ratio of
207 the measured CO₂ concentration in the intake surge tank to the CO₂ concentration in the exhaust
208 manifold.

209 **2.5 Data acquisition and analysis**

210 The instantaneous in-cylinder pressure was measured by a Kistler 6125C piezo-electric
211 pressure transducer with a sampling resolution of 0.25 CAD. The high speed and low speed
212 National Instruments data acquisition (DAQ) cards were used to acquire the high and low
213 frequency signals from the measurement devices. The captured data from the DAQ as well as
214 the resulting engine parameters were displayed in real-time by an in-house developed transient
215 combustion analysis software.

216 The crank angle based in-cylinder pressure traces were recorded through an AVL FI Piezo
217 charge amplifier, averaged over 200 consecutive engine cycles, and used to calculate the IMEP
218 and apparent heat release rate (HRR). According to [4], the apparent HRR was calculated as

$$219 \quad HRR = \frac{\gamma}{(\gamma - 1)} p \frac{dV}{d\theta} + \frac{1}{(\gamma - 1)} V \frac{dp}{d\theta} \quad (4)$$

220 where γ is defined as the ratio of specific heats, V and p are the in-cylinder volume and
221 pressure, respectively; and θ is the crank angle degree. Since the absolute value of the heat
222 release is not as important to this study as the bulk shape of the curve with respect to crank
223 angle, a constant γ of 1.33 was assumed throughout the engine cycle according to [44]. The
224 mass fraction burned (MFB) was defined by the ratio of the integral of the HRR and the
225 maximum cumulative heat release. Combustion phasing (CA50) was determined by the crank
226 angle of 50% MFB. Combustion duration was represented by the period of time between the
227 crank angles of 10% (CA10) and 90% (CA90) MFB. Ignition delay (ID) was defined as the

228 period of time between the diesel main injection timing (SOI_main) and the start of combustion
 229 (SOC), denoted as 0.3% MFB point of the average cycle. The in-cylinder combustion stability
 230 was monitored by the coefficient of variation of the IMEP (COV_IMEP) over the sampled
 231 cycles. For the sake of simplification, the average in-cylinder gas temperature was calculated
 232 by applying the ideal gas model, considering each species in the mixture.

233 Net indicated efficiency (NIE) was defined as the ratio of the work done to the rate of fuel
 234 energy supplied to the engine every cycle by

$$235 \quad NIE = \left[\frac{P_{ind}}{\dot{m}_{methanol}LHV_{methanol} + \dot{m}_{diesel}LHV_{diesel}} \right] * 100\% \quad (5)$$

236 where P_{ind} is the net indicated power in W, $\dot{m}_{methanol}$ and \dot{m}_{diesel} are the methanol and
 237 diesel mass flow rate in kg/s respectively, and LHV_{diesel} is the diesel lower heating value of
 238 42.9×10^6 J/kg.

239 The calculation of combustion efficiency was based on the unburnt exhaust products during
 240 combustion process which mainly comprised of HC and CO by

$$241 \quad Combustion\ efficiency = 1 - \frac{(ISCO LHV_{CO}) + (ISHC LHV_{DF})}{\dot{m}_{methanol}LHV_{methanol} + \dot{m}_{diesel}LHV_{diesel}} * P_i \quad (6)$$

242 where ISCO and ISHC are the net indicated specific emissions of CO and unburnt HC,
 243 respectively; LHV_{CO} is equivalent to 10.1×10^6 J/kg; The energy content of the unburnt
 244 hydrocarbons was assumed to have the lower heating value of the in-cylinder fuel mixture
 245 (LHV_{DF}).

246 **3. Methodology**

247 **3.1 Test conditions**

248 In this study, the experimental work was carried out at a speed of 1200 rpm and a high load of
249 18 bar IMEP. Table 3 summarises the engine test conditions for the CDC (diesel-only) and
250 DMDF combustion modes. The intake pressure set points of the baseline engine operation were
251 taken from a Euro V compliant multi-cylinder HD diesel engine of the same cylinder design as
252 the single cylinder engine. The exhaust pressures were adjusted to provide a constant pressure
253 differential of 0.10bar above the intake pressure, in order to realize the required EGR rate and
254 to achieve a fair comparison with equivalent pumping work.

255 A single diesel injection near firing TDC was used for the CDC and conventional DMDF
256 operations. In the advanced DMDF combustion mode, however, a small amount of pre-
257 injection fuel with an estimated volume of 3 mm³ and a constant dwell time of 1ms (e.g. 7.2
258 CAD at 1200 rpm) before main diesel injection was employed to reduce the levels of PRR. The
259 diesel main injection timings were optimised to achieve the maximum net indicated efficiency
260 in all combustion modes. The methanol energy fraction was also varied when required. The
261 P_{max} and PRR were limited to 180bar and 30bar/CAD, respectively. Stable engine operation
262 was determined by controlling the COV_{IMEP} below 3%.

263 Table 3 Engine testing conditions for CDC and DMDF operations.

Parameter	Unit	CDC operation	Conventional DMDF	Advanced DMDF
Engine load (IMEP)	bar	18		
Engine speed	rpm	1200		
Diesel injection pressure	bar	1600		

Intake air pressure	kPa	260		
Exhaust back pressure	kPa	270		
Diesel injection strategy	-	Single	Single	Pre- and main injection near TDC
Diesel SOI_main	CAD ATDC	Swept	Swept	Swept
Intake air temperature	°C	50	50	Swept
MF	%	0	Swept	Swept
EGR rate	%	0	0	Swept
Effective compression ratio	-	16.8	16.8	Swept

264

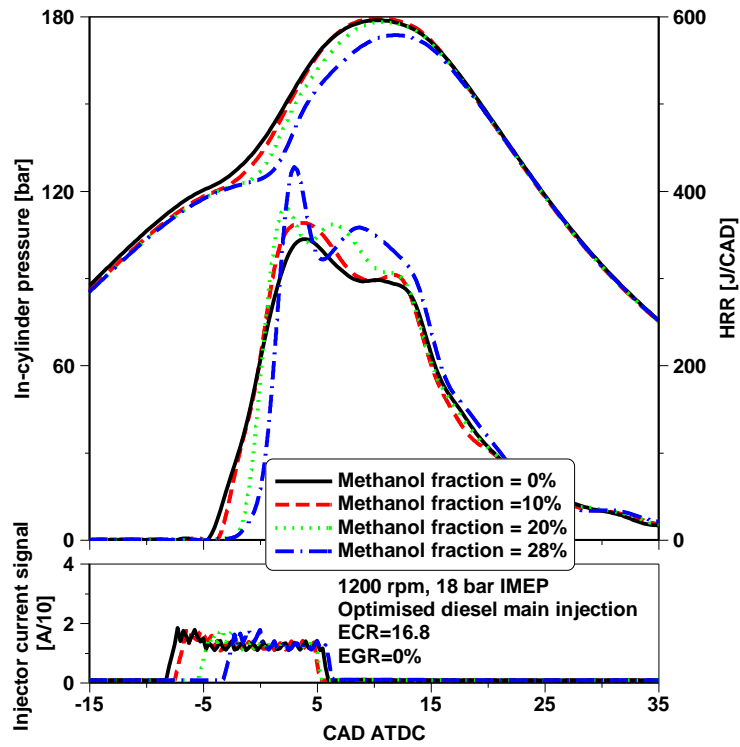
265 **4. Results and discussion**

266 **4.1 The effect of methanol energy fraction**

267 Figure 3 shows the in-cylinder pressure and HRR while Figure 4 shows the average in-cylinder
268 gas temperatures for the high load DMDF operation. The diesel SOI is an important factor in
269 maximizing engine efficiency and curbing emissions. In order to achieve high net indicated
270 efficiency, the SOI was swept for different combustion control strategies. In this study, single
271 diesel injection timing was used in a conventional DMDF engine and optimised to achieve the
272 maximum engine thermal efficiency with different methanol energy fractions varying from 0%
273 (diesel-only) to the maximum value of 28% limited by the peak cylinder pressure or heat
274 release rate.

275

276 Figure 3 and Figure 4 show that an increase in the methanol energy fraction resulted in lower
277 in-cylinder compressed gas pressure and temperature. This was mainly attributed to the two
278 following reasons. Firstly, a higher MF increased the total in-cylinder mass trapped. This was
279 attributed to the relatively lower LHV of methanol than the diesel fuel, which required more
280 methanol volume fraction to maintain the same engine output. Secondly, the cooling effect
281 achieved with higher MF due to the high latent heat of vaporization of the methanol [45]. The
282 charge cooling effect helped to decrease the charge temperature at the end of compression by
283 up to 42 K. However, it was observed that the PRR and P_{\max} increased very rapidly with higher
284 MF to exceed their limits of 180bar and 30bar/CAD if the SOI was kept constant, because of
285 the greater heat release of the increased premixed methanol charge. Therefore, the diesel
286 injection timing had to be retarded from -8 CAD ATDC to -3 CAD ATDC with higher MF in
287 order to keep the PRR and P_{\max} below their limits. It can be also seen from Figure 3 that the
288 maximum MF tends to be limited by the PRR rather than P_{\max} at a higher MF condition, as
289 suggested by the lower P_{\max} of the optimised DMDF operation with MF of 28%.



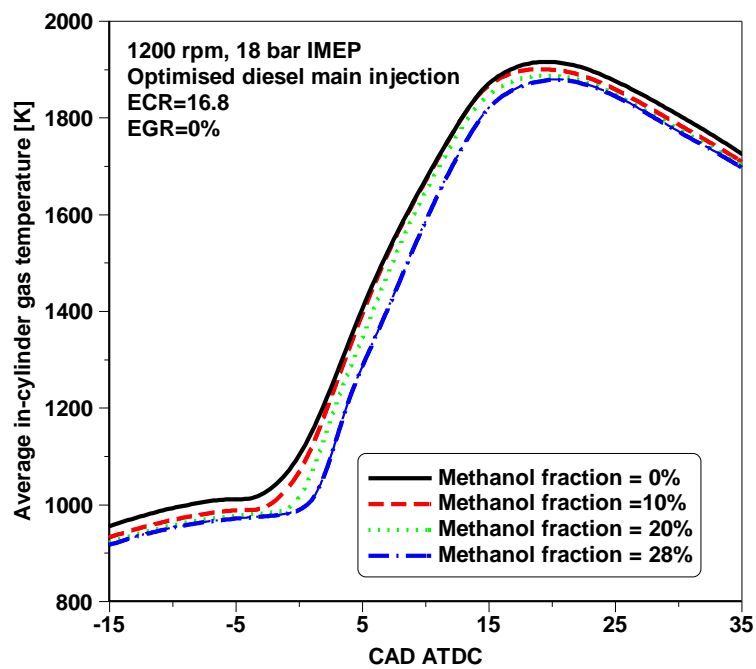
290

291

Figure 3. In-cylinder pressure, HRR, and diesel injector signal for optimised high load DMDF

292

operation with different MF.



293

294

Figure 4. Average in-cylinder gas temperature for optimised high load DMDF operation with

295

different MF.

296 As the SOI was delayed towards TDC with increased MF, the ignition delay was reduced due
 297 to higher charge temperatures as shown in Table 4, which shows the combustion characteristics,
 298 performance, and emissions of the CDC and conventional DMDF operation with different
 299 methanol energy fractions. A higher COV_{IMEP} was observed likely due to the higher peak
 300 heat release and lower local combustion temperature. The delayed combustion process as well
 301 as lower charge temperature prior to combustion decreased the average combustion gas
 302 temperature, resulting in lower NO_x emissions. The shorter ignition delay caused more
 303 diffusion burn of diesel and hence slightly higher soot emissions. The increase in the CO and
 304 HC emissions were possibly a result of more premixed fuel trapped in the crevice and squish
 305 volumes as well as more diffusion combustion of diesel and lower in-cylinder combustion
 306 temperature, yielding lower combustion efficiencies as reported in [46]. However, the
 307 reduction in heat transfer losses due to lower in-cylinder combustion temperature offset the
 308 adverse effect caused by the decreased combustion efficiency as the MF was increased from 0
 309 to 20%, resulting in a higher net indicated efficiency. When the MF was further increased to
 310 28%, however, the improvement in heat loss was weakened as more combustion was taken
 311 place in the expansion stroke. Additionally, the combustion efficiency was further decreased.
 312 These effects resulted in a lower net indicated efficiency when operating DMDF with MF of
 313 28% than MF of 20%.

314 Table4. The effect of MF on optimised high load conventional DMDF operation with single
 315 diesel injection.

Parameter	Unit	MF=0%	MF=10%	MF=20%	MF=28%
Diesel SOI	CAD ATDC	-8	-7.25	-5.25	-3
COV _{IMEP}	%	0.40	0.54	1.08	1.67
PRR	bar/CAD	19.2	24.5	28.4	29.6
P _{max}	bar	180.1	179.5	179.0	174.4

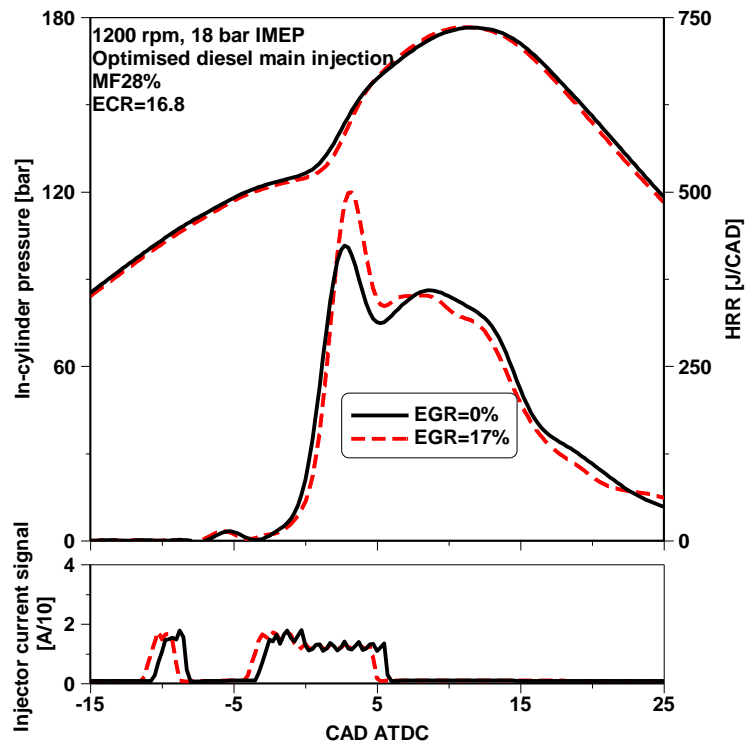
Ignition delay (SOC-SOI)	CAD	5.0	4.6	3	0.75
CA50	CAD ATDC	9.0	8.8	9.0	10.0
CA10-CA90	CAD	21.5	21.3	20.9	20.4
Lambda	-	1.98	2.04	2.09	2.11
ISsoot	g/kWh	0.0013	0.0015	0.0017	0.0018
ISNO _x	g/kWh	17.5	16.5	14.3	12.7
ISCO	g/kWh	0.1	1.4	2.9	3.6
ISHC	g/kWh	0.13	0.45	0.99	1.54
Combustion efficiency	%	99.9	99.5	99.0	98.6
NIE	%	45.3	45.7	46.1	45.79

316

317 **4.2 The effect of EGR**

318 Following the studies on the conventional DMDF combustion with a single diesel injection,
319 the pilot injection was introduced and found to be effective to reduce PRR and P_{max} , as can be
320 seen in the results of 28% MF in Tables 3 and 4. The pilot injection was kept constant at 3 mm³
321 with a constant dwell time of 1ms. This section presents the experimental results in terms of
322 the effect of EGR on the optimised DMDF combustion with the pilot injection. The boundary
323 conditions were held constant and the MF was maintained at 28%. Figure 5 shows the in-
324 cylinder pressure, diesel injection, and HRR curves of the optimum DMDF operation at 0%
325 and 17% EGR. The decreased oxygen concentration and increased heat capacity of the in-
326 cylinder charge with the use of EGR increased the main injection delay, allowing for a more
327 advanced diesel SOI_{main} to optimise the engine efficiency. It can be seen that there was a
328 small heat release of the pre-injected diesel occurred prior to the main diesel injection in both
329 operations with and without EGR. With EGR the ignition delays for both pilot injection and

330 main diesel injection were slightly longer than those without EGR, resulting in the slightly
331 higher percentage of premixed combustion in the first heat release peak with EGR.



332

333 Figure 5. In-cylinder pressure, HRR, and diesel injector signal for optimised high load DMDF
334 operation with and without EGR.

335 Table 5 summarises the resulting performance and emissions results of the optimised DMDF
336 operation with and without EGR. The addition of EGR delayed the combustion process and
337 increased the combustion duration, despite the CA50 was maintained similar to the case
338 without EGR by an advanced diesel SOI_{main}. The NO_x emissions were drastically reduced
339 from 12.9 to 4.4 g/kWh while the soot emissions were slightly increased due to the lower
340 combustion temperature and a reduction in in-cylinder lambda. The longer mixing period and
341 lower lambda contributed to a small decrease in CO and HC emissions and thus slightly higher
342 combustion efficiency. Net indicated efficiency with EGR was higher than that without EGR,
343 which possibly was a result of higher peak heat release, slightly higher combustion efficiency,
344 and lower combustion temperature.

Table5. The effect of EGR on optimised high load DMDF operation with pilot injection.

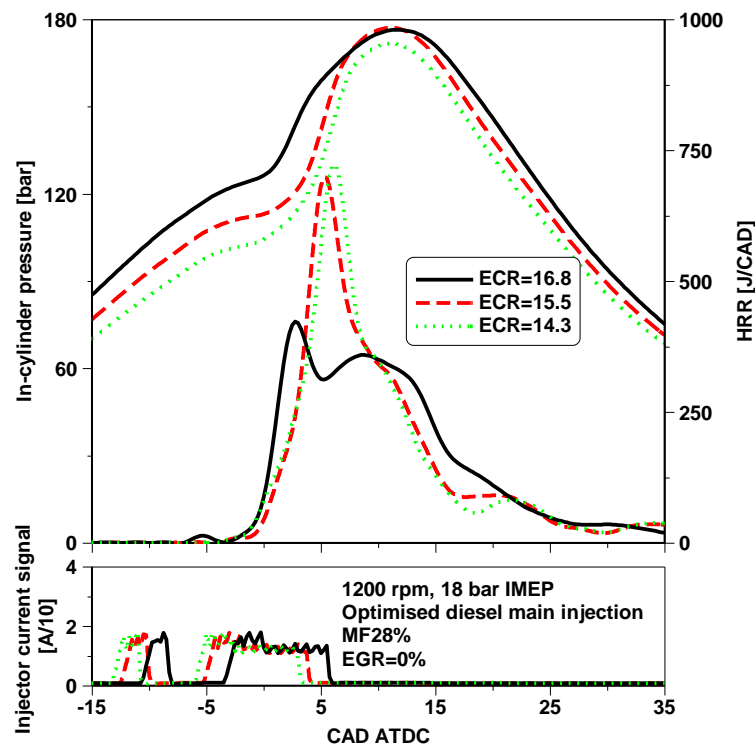
Parameter	Unit	EGR=0%	EGR=17%
MF	%	28	28
Diesel SOI_main	CAD ATDC	-3.25	-4.0
COV_IMEP	%	1.66	1.60
PRR	bar/CAD	23.5	24.1
P _{max}	bar	178	178
Ignition Delay (main)	CAD	0.75	1.6
CA50	CAD ATDC	9.5	9.3
CA10-CA90	CAD	20.1	21.8
Lambda	-	2.1	1.7
ISsoot	g/kWh	0.0013	0.0019
ISNO _x	g/kWh	12.9	4.4
ISCO	g/kWh	3.6	3.4
ISHC	g/kWh	1.6	1.3
Combustion efficiency	%	98.5	98.9
NIE	%	46.15	46.57

346

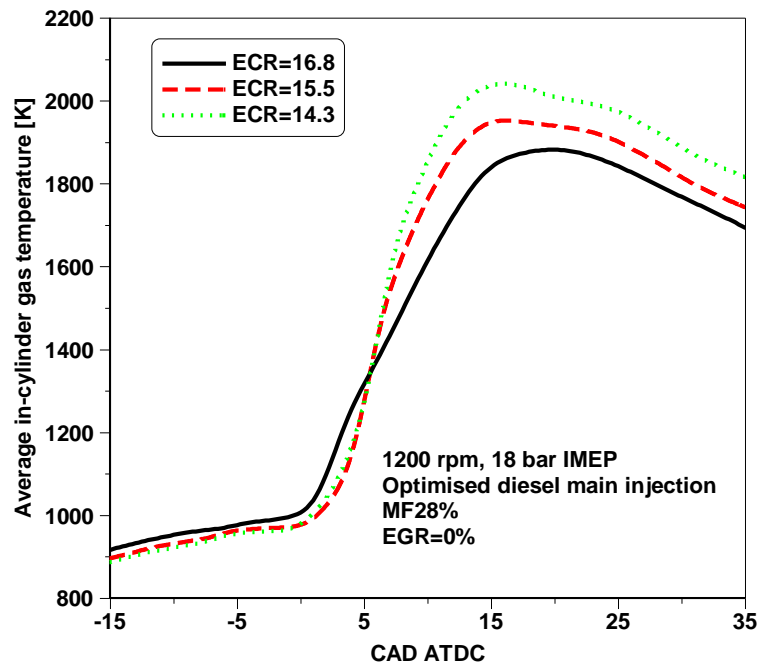
347 **4.3 The effect of Miller cycle**

348 The Miller cycle was employed in this section in an attempt to minimise the PRR and the in-
349 cylinder pressure to enable a more advanced combustion phasing for improving upon engine
350 efficiency. Figure 6 depicts the effect of DMDF operation with different ECR on the heat
351 release characteristics. The methanol energy fraction was maintained at 28% and the diesel
352 main injection timings were optimised up to the PRR or peak in-cylinder pressure limitations.

353 The decreased ECR via LIVC effectively reduced the compressed gas pressure and temperature
 354 before combustion as shown in Figure 7. This successfully delayed the ignition and combustion
 355 of the premixed fuel and thus suppressed the PRR and P_{max} , allowing for a much more advanced
 356 diesel SOI_main to optimise the engine efficiency. The two distinct heat release events in the
 357 baseline ECR of 16.8 disappeared when operating with a lower ECR. This was a result of the
 358 increased mixing period during the ignition period and thus a more homogeneous combustion
 359 as supported by the significantly higher peak heat release. A reduction in ECR led to higher
 360 average in-cylinder gas temperature during combustion attributed to a decrease in the in-
 361 cylinder mass trapped and therefore decreased the total heat capacity of gases. The reason for
 362 the slightly lower P_{max} in the ECR of 14.3 was due to the high level of PRR, which limited the
 363 optimisation of diesel injection timing. It is noted that a small amount of heat release from the
 364 pre-injected diesel occurred before diesel SOI_main at the ECR of 16.8 was successfully
 365 prevented by lowering the ECR. This was a result of the decreased compressed gas temperature,
 366 which avoid the heat release of the premixed charge.



368 Figure 6. In-cylinder pressure, HRR, and diesel injector signal for optimised high load DMDF
 369 operation with different ECR.



370
 371 Figure 7. Average in-cylinder gas temperature for optimised high load DMDF operation with different
 372 ECR.

373 Table 6 shows the resulting combustion characteristics, performance, and emissions of the
 374 optimised DMDF operation with different ECR. As the ECR decreased, the optimum diesel
 375 main injection was advanced. This resulted in an increase in PRR while had less impact on
 376 combustion characteristics and engine emissions. Additionally, the lower ECR slightly
 377 improved the combustion efficiency, which along with the resulting faster HRR contributed to
 378 the improvement in engine thermal efficiency.

379 Table 6. The effect of EGR on optimised high load DMDF operation.

Parameter	Unit	ECR=16.8	ECR=15.5	ECR=14.3
MF	%	28	28	28
Diesel SOI_main	CAD ATDC	-3.25	-5	-5.75

Ignition Delay (main)	CAD	0.75	3.3	3.9
COV_IMEP	%	1.66	1.46	1.66
PRR	bar/CAD	23.5	28.5	29.4
P_{max}	bar	178	178.5	174
CA50	CAD ATDC	9.5	8.0	8.0
CA10-CA90	CAD	20.1	19.0	20.2
Lambda	-	2.1	1.9	1.7
ISoot	g/kWh	0.0013	0.0010	0.0012
ISNO _x	g/kWh	12.9	13.3	12.2
ISCO	g/kWh	3.6	3.1	2.7
ISHC	g/kWh	1.6	1.2	2.7
Combustion efficiency	%	98.5	98.9	99.2
NIE	%	46.15	46.23	46.41

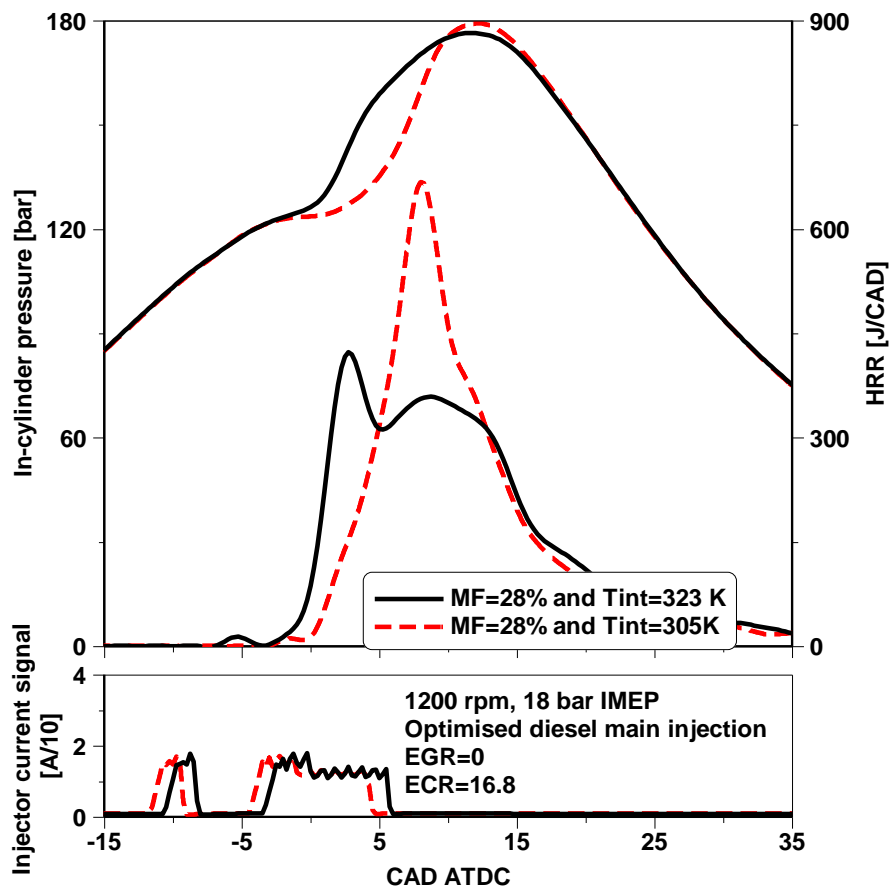
380

381 **4.4 The effect of intake air cooling**

382 The last approach used in this study to control the PRR and P_{max} of the DMDF combustion is
383 the intake air cooling. The experiments were performed without EGR at the baseline ECR of
384 16.8. The diesel injection timings were optimised and the MF was maintained at 28%. The
385 intake air temperature (T_{int}) was controlled by using an air-to-water cooler and an intake air
386 heater.

387 Figure 8 shows the in-cylinder pressure, diesel injection, and HRR curves of the optimised
388 DMDF operation with a pilot injection at different intake air temperatures. A reduction in the
389 T_{int} from 323 to 305 K effectively decreased the average in-cylinder gas temperature by 50 K
390 during the compression process, as demonstrated in Figure 9. Therefore, the ignition delay of

391 the premixed charge was increased to allow for an advanced diesel SOI_{main} to be used. The
 392 decreased compressed gas temperature also prevented the autoignition and heat release of the
 393 premixed fuel prior to the diesel SOI_{main}. The in-cylinder gas pressure during compression
 394 stroke was similar to that with higher T_{int} of 323 K due to the balance effect between the lower
 395 compressed gas temperature and the resulting higher in-cylinder gas density. The longer mixing
 396 period noticeably increased the peak heat release while the delayed combustion process and
 397 decreased compressed gas temperature contributed to a reduction in the average in-cylinder gas
 398 temperature during the combustion process.



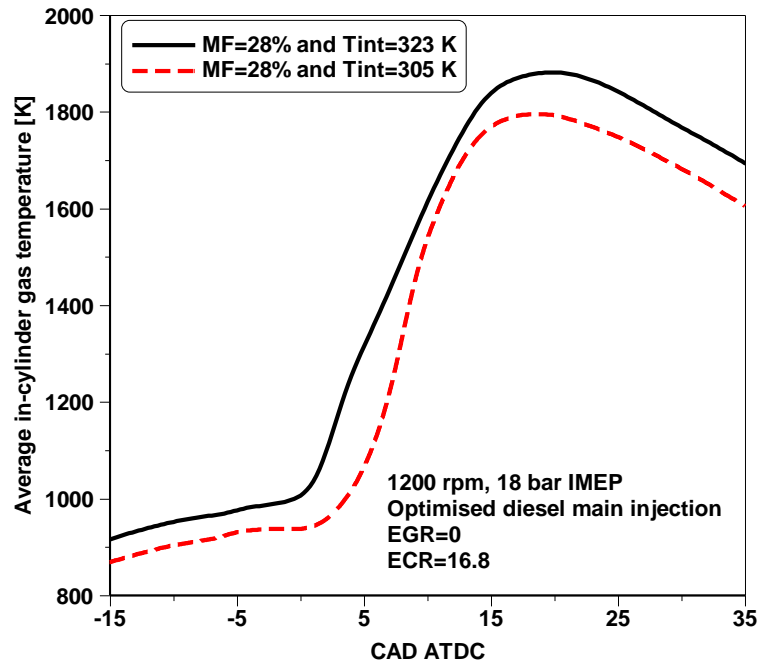
399

400 Figure 8. In-cylinder pressure, HRR, and diesel injector signal for optimised high load DMDF

401

operation with different T_{int} and MF.

402



403

404 Figure 9. Average in-cylinder gas temperature for optimised high load DMDF operation with different
 405 T_{int} and MF.

406 The combustion characteristics, performance and emissions results of the optimised DMDF
 407 operation with different intake coolant temperatures are summarised in Table 7. Compared to
 408 the higher T_{int} , the DMDF operation with a lower T_{int} advanced the optimum diesel main
 409 injection timing while reducing the level of PRR. The reduction in T_{int} with optimised diesel
 410 main injection timing produced slight impact the combustion characteristics and emissions.
 411 The resulting higher degree of premixed combustion and lower average in-cylinder gas
 412 temperature promoted the engine thermal efficiency from 46.15% to 47.05%.

413

Table7. The effect of EGR on optimised high load DMDF operation.

Parameter	Unit	$T_{int}=323K$	$T_{int}=305K$
MF	%	28	28
Diesel SOI_main	CAD ATDC	-3.25	-4.25
Ignition Delay (main)	CAD	0.75	4.1

COV_IMEP	%	1.66	1.84
PRR	bar/CAD	23.5	18.9
P _{max}	bar	178	180
CA50	CAD ATDC	9.5	9.6
CA10-CA90	CAD	20.1	18.1
Lambda	-	2.1	2.2
ISsoot	g/kWh	0.0013	0.0014
ISNO _x	g/kWh	12.9	12.7
ISCO	g/kWh	3.6	5.3
ISHC	g/kWh	1.6	1.9
Combustion efficiency	%	98.5	98.2
NIE	%	46.15	47.05

414

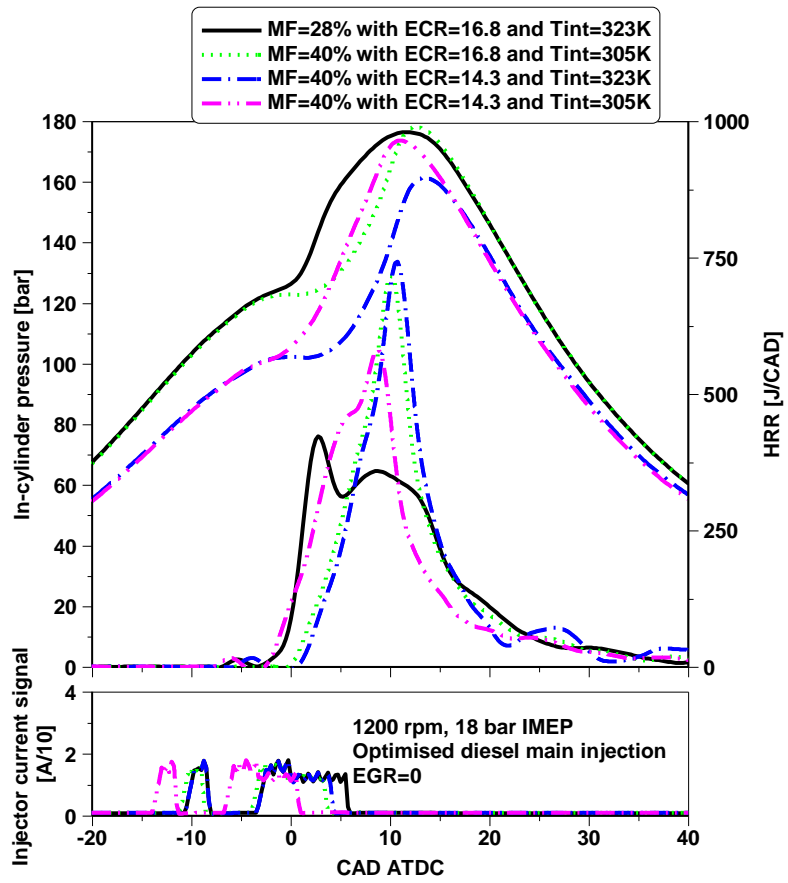
415 **4.5 Analysis of DMDF operation with combined Miller cycle and intake air**
416 **cooling**

417 This subsection aims to analyse the effect of the DMDF operation with both Miller cycle and
418 intake air cooling on combustion process and explore their potential for increasing the
419 maximum net indicated efficiency. A pre-injection with an estimated volume of 3 mm³ and a
420 constant dwell time of 7.2 CAD to the diesel main injection was introduced. The diesel
421 injection timings were adjusted for engine operations with ECR of 16.8 and 14.3 and methanol
422 energy fractions of 28% and 40%. The operation with a limited MF of 28% at an ECR of 16.8
423 and T_{int} of 323 K was taken as the reference and no EGR was used.

424 **4.5.1 Combustion characteristics of DMDF operation with Miller cycle and intake air** 425 **cooling**

426

427 Figure 10 shows the in-cylinder pressure, diesel injection, and HRR curves of the different
428 optimised DMDF combustion modes. A higher MF of 40% can be obtained when applying
429 Miller cycle or intake air cooling strategies. Figure 11 depicts that the use of Miller cycle and
430 lower T_{int} with a higher MF effectively decreased the average in-cylinder gas temperature
431 during compression stroke, reducing up to nearly 90 K in their combination when compared to
432 the baseline operation. This substantially delayed the ignition timing of the premixed charge
433 and potentially minimised the PRR and P_{max} , allowing for a more advanced diesel injection
434 timing to improve upon the engine efficiency. As a consequence, the longer premixed period
435 and relatively higher MF significantly increased the peak heat release. The compressed gas
436 pressure was decreased by the lower ECR, which was not achievable by the use of a lower T_{int} .
437 This was primarily attributed to the increased in-cylinder gas density, as to be demonstrated in
438 the later part of this section. A relatively lower peak in-cylinder pressure observed in the
439 operation with MF of 40% at an ECR of 14.3 and T_{int} of 323 K was because the main diesel
440 injection timing was limited by higher levels of the PRR. Moreover, the average in-cylinder
441 gas temperature during combustion process was increased in the lower ECR cases due to the
442 lower in-cylinder mass trapped while was decreased in the lower T_{int} at an ECR of 16.8, which
443 was attributed to the higher in-cylinder charge mass and lower compressed gas temperature.



444

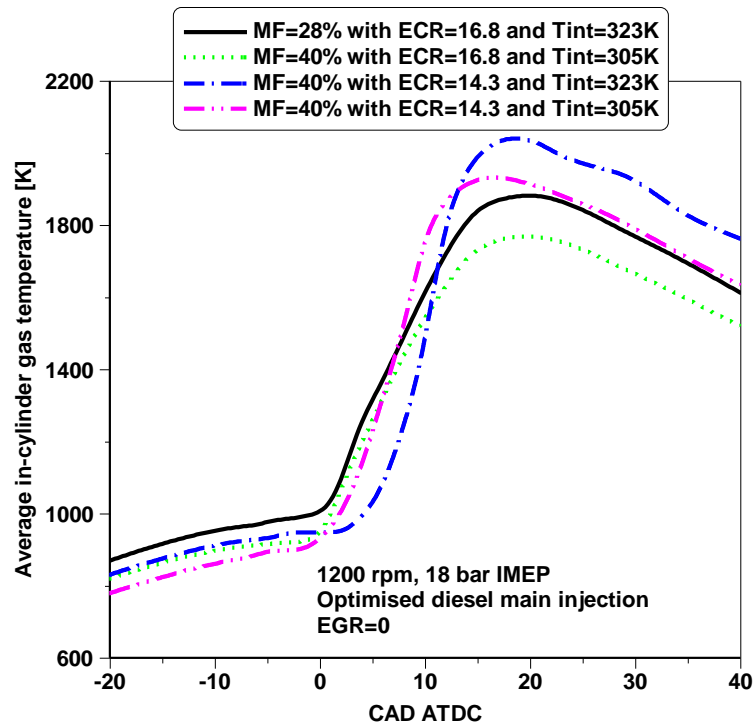
445

Figure 10. In-cylinder pressure, HRR, and diesel injector signal for optimised high load DMDF

446

operation with Miller cycle and intake air cooling.

447

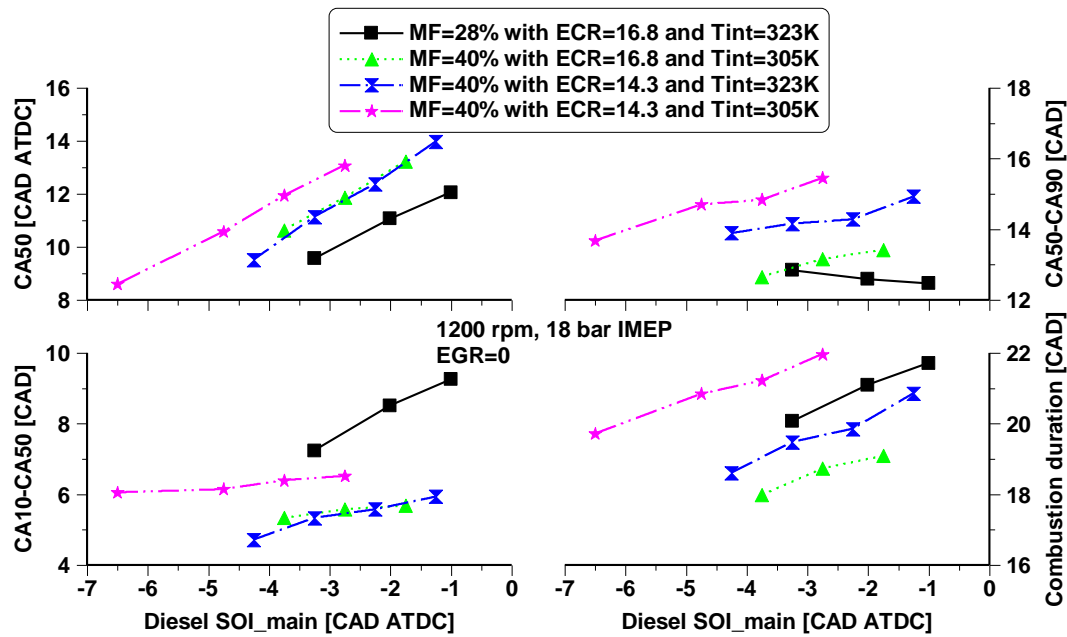


448

449 Figure 11. Average in-cylinder gas temperature for optimised high load DMDF operation with Miller
450 cycle and intake air cooling.

451 Figure 12 shows the combustion characteristics as a function of the diesel SOI_{main} for
452 different DMDF combustion modes. For a constant diesel SOI_{main} with MF of 40%, the
453 CA50 (e.g. combustion phasing) was delayed by a lower ECR and T_{int} because of the delayed
454 combustion process. However, much earlier diesel SOI_{main} enabled by the combined lower
455 ECR and lower T_{int} advanced the combustion process. The higher degree of premixed
456 combustion with the use of lower ECR and lower T_{int} accelerated the initial combustion, as
457 evidenced by a shorter period of CA10-CA50 than that of the baseline operation. On the
458 contrary, the weakened mixing-control combustion lengthened the late combustion process as
459 measured by a longer period of CA50-CA90. As a consequence, the period of CA10-CA90
460 (e.g. combustion duration) for the DMDF operation with 40% MF was shortened when diesel
461 SOI_{main} was optimised for the lower ECR or lower T_{int} . As shown in Figure 10, however,
462 the combustion duration was longer if the diesel SOI_{main} was kept constant when the ECR

463 or/and T_{int} were decreased. This was mainly attributed to the slower mixing-controlled
 464 combustion, which was supported by the decreased heat release of the late combustion phase.



465
 466 Figure 12. Combustion characteristics for optimised high load DMDF operation with Miller cycle and
 467 intake air cooling.

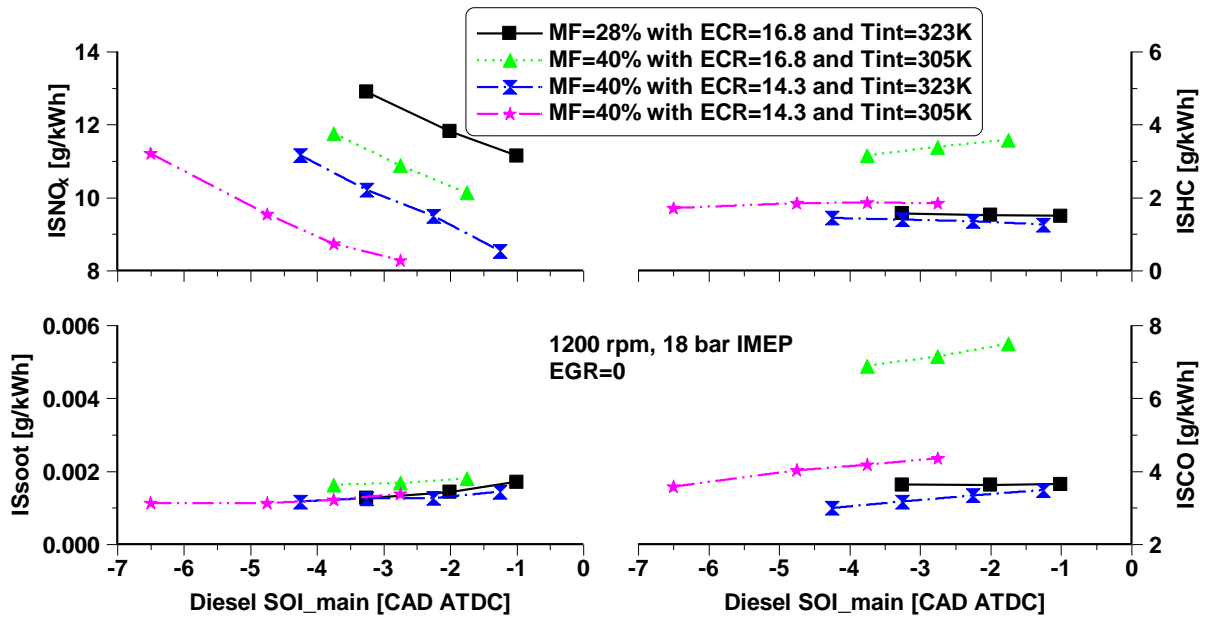
468 **4.5.2 Exhaust emissions and performance of DMDF operation with Miller cycle and**
 469 **intake air cooling**

470 Figure 13 and Figure 14 depict the net indicated specific emissions and engine performance
 471 versus the diesel SOI_main respectively for the different combustion modes. The DMDF
 472 operation with higher MF at a lower ECR and T_{int} achieved a significant reduction in NO_x
 473 emissions. This was likely a result of the more homogeneous combustion as less diesel fuel
 474 was burned during the mixing-controlled combustion process and the lower compressed gas
 475 temperature caused by Miller cycle and intake air cooling, which led to a lower peak
 476 combustion temperature. In particular, the cases with Miller cycle yielded lower NO_x emissions,
 477 which associated with the lower in-cylinder lambda as demonstrated in Figure 14. Miller cycle,
 478 intake cooling, and a higher MF produced little impact on the soot emissions. All soot

479 emissions were below 0.002 g/kWh, which was well below than the Euro VI particulate matter
480 limit of 0.01 g/kWh even without the diesel particulate filter [47].

481 The CO and HC emissions were substantially increased as more methanol was injected at a
482 lower T_{int} of 305 K. This phenomenon was likely attributed to the increased premixed
483 methanol-air mixture trapped in the squish and crevice regions as reported in [19,46].
484 Additionally, the decreased in-cylinder gas temperature was also play an important role on the
485 increase in HC and CO emissions. As a result, the combustion efficiency was reduced. The use
486 of Miller cycle helped to suppress the HC and CO emissions, especially when operating at a
487 higher T_{int} of 323 K. This was possibly a result of the lower in-cylinder compression pressure,
488 which minimised the amount of premixed fuel pressed into the squish and crevice regions.
489 Apart from that, the faster HRR and higher in-cylinder fuel-air ratio increased the mean in-
490 cylinder gas temperatures during combustion, which probably was one of the reasons for a
491 reduction in HC and CO emissions as it could help to improve the oxidation of HC and CO
492 emissions [48]. Consequently, this allowed for higher combustion efficiency than those
493 achieved with reference case.

494 The use of Miller cycle and intake air cooling at a higher MF decreased the levels of PRR,
495 which was linked to the reduction in compression temperatures. Figure 14 also revealed that a
496 reduction in the T_{int} increased the net indicated efficiency at the optimised diesel SOI_{main},
497 especially when combining with Miller cycle. This was likely a result of more homogeneous
498 combustion and lower heat transfer losses resulted from the lower local combustion
499 temperature. However, the use of Miller cycle with MF of 40% at a higher T_{int} slightly
500 decreased the net indicated efficiency despite a small increase in combustion efficiency. This
501 was possibly due to the decreased in-cylinder lambda and a higher average in-cylinder gas
502 temperature during combustion, which could increase the heat losses.



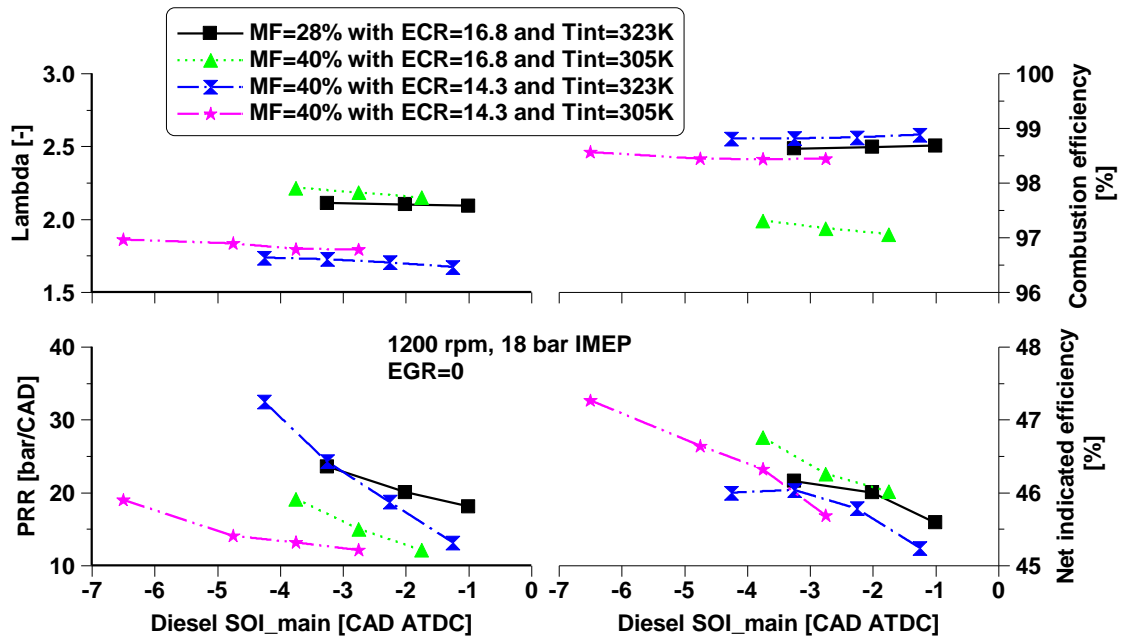
503

504

Figure 13. Net indicated specific emissions for optimised high load DMDF operation with Miller cycle and intake air cooling.

505

506



507

508

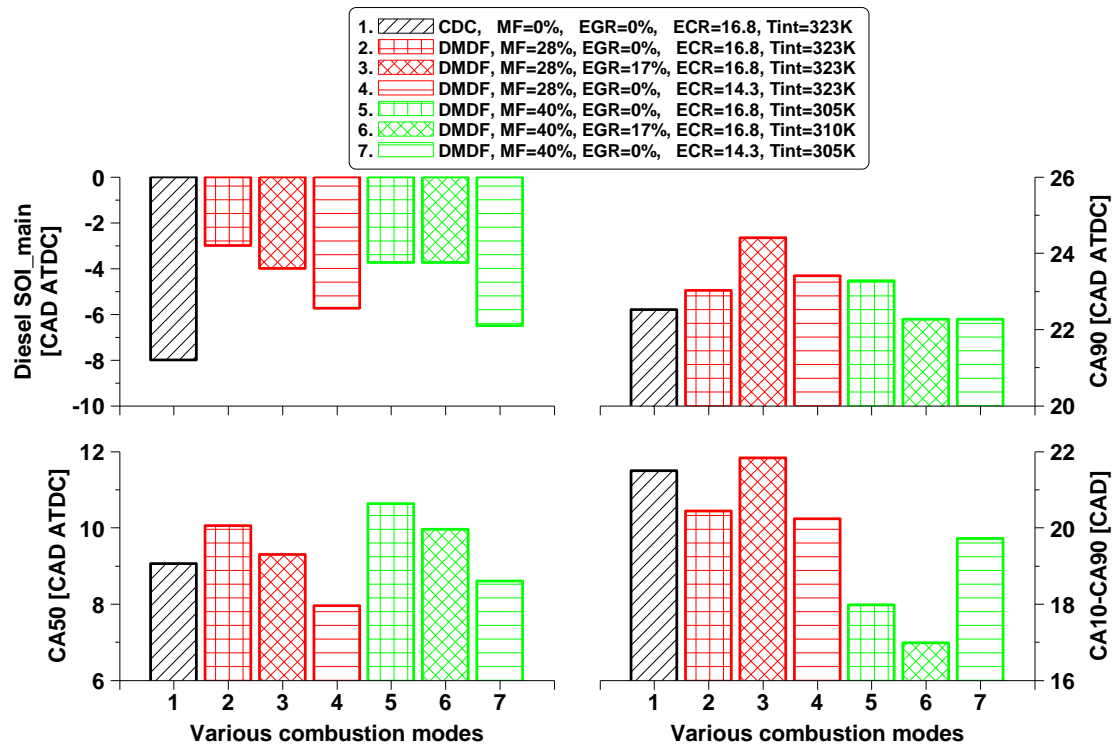
Figure 14. Engine performance for optimised high load DMDF operation with Miller cycle and intake air cooling.

509

510 **4.6 Comparison of different engine combustion modes**

511 This subsection performs a comparison of the different combustion modes in terms of
512 combustion characteristics, engine-out emissions, and performance, in order to explore
513 advanced combustion control strategies for efficient high load DMDF operation.

514 Figure 15 shows the optimised diesel SOI_{main} and combustion characteristics for the CDC
515 (e.g. black bar) and DMDF operation with lower MF of 28% at higher T_{int} of 323 K (e.g. red
516 bar) and with higher MF of 40% at lower T_{int} conditions (e.g. green bar). It should be note that
517 the use of recycled exhaust gas limited the lowest intake air temperature to 310 K when
518 operating with an EGR rate of 17%. Compared to the CDC, the optimised diesel SOI_{main}
519 was delayed in the DMDF operation in order to avoid excessive PRR and peak in-cylinder
520 pressure limit. This delayed the CA50 and CA90, but the period of CA10-CA90 was decreased
521 due to a more homogeneous combustion than that of the CDC. The use of EGR and Miller
522 cycle enabled an earlier diesel injection timing, which helped to advance the CA50. However,
523 the DMDF operation with EGR at a higher T_{int} lengthened the mixing-control combustion as
524 measured by a later CA90. This was the reason for a longer period of CA10-CA90. At a lower
525 T_{int}, however, the DMDF operation with EGR achieved shorter period of CA10-CA90 than
526 those attained without EGR. This phenomenon was possibly linked to the relatively higher T_{int}
527 by 5 K when operating with EGR of 17%, which accelerated the combustion process. Overall,
528 the DMDF operation with higher MF at a lower T_{int} allowed for relatively advanced diesel
529 injection timing and shorter CA10-CA90 than those with a lower MF at a higher T_{int}.



530

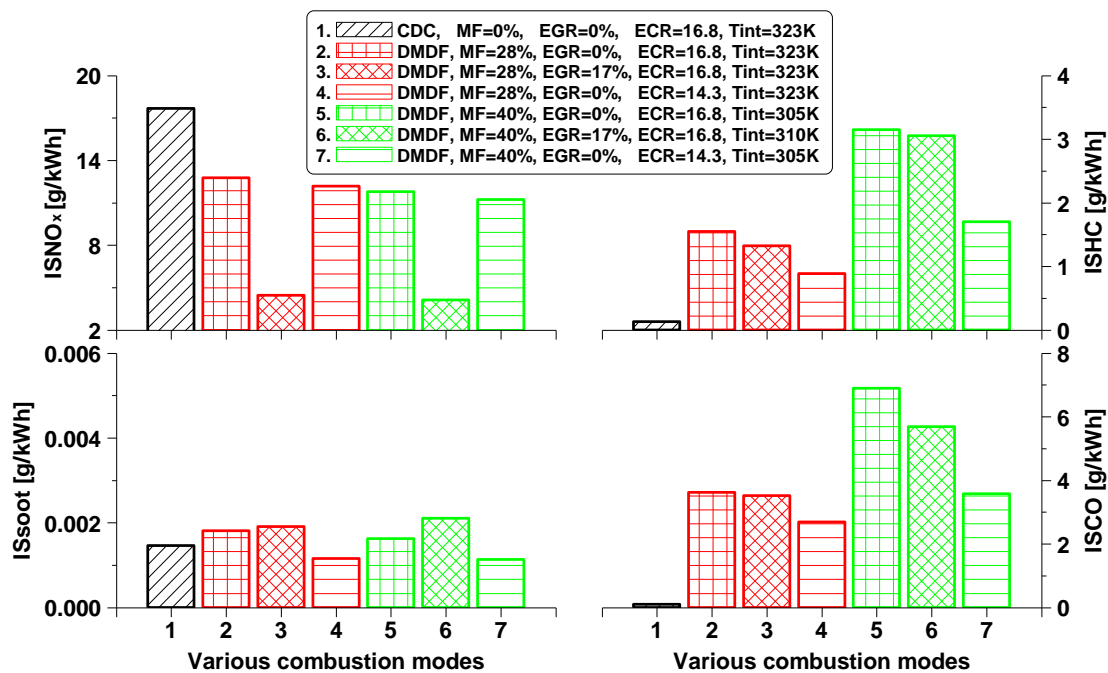
531 Figure 15. Comparison of main diesel injection timing and combustion characteristics for optimised
 532 CDC and DMDF operations.

533

534 Figure 16 depicts the net indicated specific emissions for the most efficient cases in different
 535 combustion modes. The DMDF operation achieved lower NO_x emissions than the CDC,
 536 reducing NO_x emissions from 17.5 g/kWh in the CDC operation to 12.7 g/kWh in the DMDF
 537 operation with MF of 28%. The use of EGR decreased the in-cylinder oxygen availability and
 538 increased the total gas heat capacity, yielding further significantly lower NO_x emissions. As a
 539 result, the introduction of EGR decreased NO_x emissions from 12.7 to 4.4 g/kWh and 11.7 to
 540 4.1 g/kWh (e.g. 65% reduction) under DMDF operation with MF of 28% and 40%, respectively.
 541 Additionally, the optimised DMDF operation with Miller cycle and intake air cooling obtained
 542 a slight reduction in NO_x emissions to 11.2 g/kWh. The variations in soot emissions were
 543 insignificant in all combustion modes, maintaining a very low level of less than 0.002 g/kWh,
 544 which is well below Euro VI particulate matter limit even without the diesel particulate filter.
 545 However, the DMDF operation apparently increased the CO and HC emissions, which was a

546 result of the occurrence of the premixed fuel trapped in the squish and crevice volumes.
 547 Particularly when operating with a higher MF at a lower intake air temperature, the CO and
 548 HC emissions were much higher. The lower average in-cylinder gas temperature during
 549 combustion also contributed to an increase in the CO and HC emissions. It can be also seen
 550 that the use of Miller cycle helped to minimise the CO and HC emissions due to the increased
 551 combustion temperature.

552



553

554 Figure 16. Comparison of Net indicated specific emissions for optimised CDC and DMDF operations.

555

556 Figure 17 depicts a comparison of engine performance between the CDC and DMDF operation
 557 with lower MF at a higher T_{int} and with a higher MF at a lower T_{int} conditions, respectively.
 558 The baseline DMDF operation at an ECR of 16.8 without EGR increased the in-cylinder
 559 lambda compared to the CDC. The application of Miller cycle and EGR clearly decreased the
 560 in-cylinder lambda. A reduction in the T_{int} substantially decreased the levels of PRR compared
 561 to those with higher T_{int} at the most efficient cases. This also revealed that the limitation for

562 the improvement in engine efficiency was the P_{\max} rather than the PRR when operating the
563 high load DMDF with intake air cooling. It can be also seen that the PRR of the DMDF
564 operation with EGR at a higher T_{int} was relatively lower. This was due to the later optimised
565 diesel SOI_{main}, which was constrained by the P_{\max} . However, the PRR was relatively higher
566 when the DMDF operation with EGR at a lower T_{int} condition. This was a result of the
567 relatively higher T_{int} by 5 K when introducing the recycled exhaust gas, which advanced the
568 ignition timing of the premixed charge.

569 The increased HC and CO emissions in the DMDF operation (as shown in Figure 16) was the
570 reason for the decrease in the combustion efficiency, particularly at a higher MF and lower
571 intake air temperature. The DMDF operation obtained higher net indicated efficiency than the
572 CDC due to more homogeneous combustion with lower heat transfer losses. This was become
573 more obvious at the lower T_{int} . There were also exceptions when operating DMDF with EGR
574 at the lower T_{int} , the net indicated efficiency was much lower possibly linked to the relatively
575 higher T_{int} of 310 K. The leaner DMDF operation with MF of 40% at an ECR of 14.3 and T_{int}
576 of 305 K allowed for more advanced CA50 and higher peak heat release. Therefore, the net
577 indicated efficiency was increased from 45.7% of the CDC and 46.2% of the DMDF with 28%
578 MF to the highest of 47.4% of the optimised DMDF with a higher MF of 40% and lower ECR
579 without EGR. Although the DMDF operation with EGR can potentially achieve low levels of
580 NO_x emissions, the use of recycled exhaust gas limited the intake air temperature control, which
581 inhibited the improvement in the net indicated efficiency (46.0%).

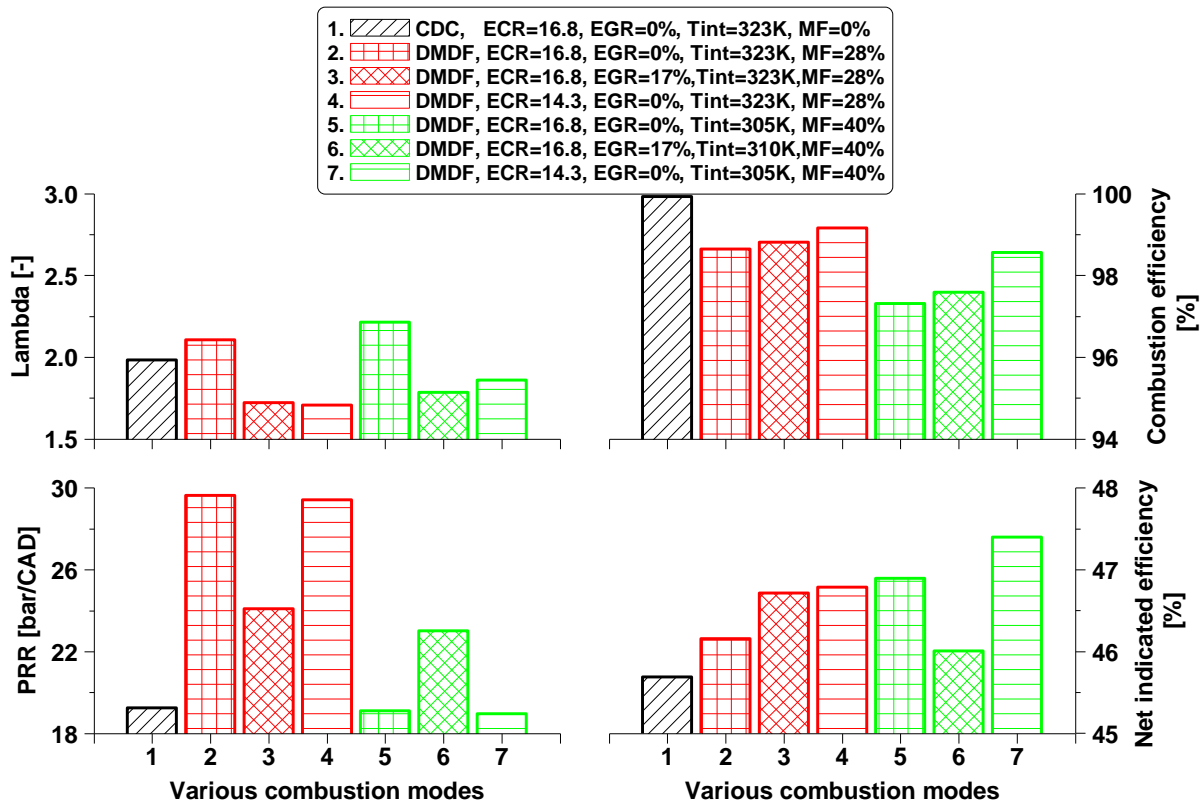


Figure 17. Comparison of engine performance for optimised CDC and DMDF operations.

5. Conclusions

In this study, systematic experiments were performed on a heavy-duty diesel engine operating at a high engine load of 18 bar IMEP with the aim to improve the high load diesel-methanol dual-fuel operation in terms of the percentage of methanol as well as the engine performance and emissions. Miller cycle, EGR, and intake air cooling achieved were investigated as effective combustion control strategies for extending the DMDF operation with higher methanol energy fraction and increasing the net indicated efficiency. The effect of the Miller cycle combined with lower intake air temperature on the combustion characteristics, exhaust emissions, and performance of the DMDF operation was also analysed. Finally, a comparison of the different combustion control strategies for the DMDF operation was performed to

595 quantify their potential benefit compared to the conventional diesel combustion. The primary
596 findings can be summarised as follows:

- 597 1. In the high load engine operation, a higher level of pressure rise rate was observed as the
598 methanol energy fraction was increased. As such, the limitation for engine efficiency
599 improvement was transferred from the P_{max} encountered in the CDC to the PRR in the
600 DMDF combustion. This was a result of a faster and more homogeneous combustion
601 occurred in the DMDF combustion with a limited MF to 28%.
- 602 2. The introduction of EGR of 17% demonstrated very little impact on the ignition timing of
603 the premixed charge as evidenced by the existence of the two distinct heat release events.
604 This was likely attributed to the insignificant impact on the in-cylinder gas temperature
605 during compression.
- 606 3. The application of Miller cycle via LIVC and the reduction in intake air temperature via an
607 air-to-water heat exchanger demonstrated the potential for higher methanol substitution
608 ratios as it apparently decreased the in-cylinder gas temperature during compression. This
609 successfully delayed the ignition timing of the premixed charge and thus decreased the
610 levels of PRR and P_{max} , allowing for a better combustion control.
- 611 4. The combination of Miller cycle and intake air cooling effectively improved the DMDF
612 operation to a higher MF of 40% by keeping PRR below the limit through the optimised
613 diesel injection timing. The resulting more homogeneous combustion and lower heat
614 transfer losses resulted from the lower local combustion temperature decreased the NO_x
615 emissions and increased the net indicated efficiency.
- 616 5. The high load DMDF combustion decreased the average in-cylinder gas temperature,
617 allowing for a reduction in heat transfer loss at the expense of lower combustion efficiency
618 when compared to the CDC. Consequently, the overall engine efficiency was the

619 counterbalance result between the improvement in heat transfer losses and the penalty in
620 combustion efficiency.

621 6. The optimised DMDF combustion attained higher net indicated efficiency than the CDC.
622 This improvement became more obvious when operating at a lower intake air temperature
623 despite lower combustion efficiency. The lower T_{int} also helped to minimise the levels of
624 PRR in the optimised DMDF operation with or without using Miller cycle or EGR when
625 compared to those at higher T_{int} .

626 7. Optimised DMDF operation with EGR of 17% and MF of 40% at a lower T_{int} condition
627 achieved the lowest NO_x emissions of 4.1 g/kWh. However, the improvement in thermal
628 efficiency was inhibited by the intake air temperature control as the use of recycled exhaust
629 gas limited the intake air temperature to 310 K.

630 8. Preferably, the optimised DMDF operation with Miller cycle (e.g. ECR=14.3) and MF of
631 40% at a lower T_{int} attained the highest net indicated efficiency of 47.4%, which was
632 increased by 3.7% and 2.6% respectively when compared to the optimised CDC (45.7%)
633 and conventional DMDF (46.2%). This improvement was accompanied with a reduction
634 of 37% in NO_x emissions and little impact on soot emissions in comparison with the CDC.

635 Overall, this work evidences the ignition timing of the premixed methanol is closely related to
636 the compression temperature and demonstrates the potential of Miller cycle and intake air
637 cooling as effective combustion control strategies for in-cylinder gas temperature control and
638 thus to achieve efficient high load DMDF operation with the greater use of methanol.

639 **Contact information**

640 Dr Wei Guan

641 Email: gwei916@163.com

642 or

643 Professor Hua Zhao

644 Email: hua.zhao@brunel.ac.uk
645 Centre for Advanced Powertrain and Fuels Research
646 College of Engineering, Design and Physical Sciences
647 Brunel University London
648 Kingston Lane
649 Uxbridge
650 Middlesex UB8 3PH
651 United Kingdom

652 **Acknowledgments**

653 Dr Wei Guan would like to acknowledge the Guangxi Yuchai Machinery Company for
654 supporting his PhD study supervised by Prof. Hua Zhao at Brunel University London.

655 **Declaration of conflicting interests**

656 The author(s) declared no potential conflicts of interest with respect to the research, authorship,
657 and/or publication of this article.

658 **Definitions/Abbreviations**

ATDC	After Firing Top Dead Center.
CA90	Crank Angle of 90% Cumulative Heat Release.
CA50	Crank Angle of 50% Cumulative Heat Release.
CA10	Crank Angle of 10% Cumulative Heat Release.
CA10-CA50	10–50% Cumulative Heat Release.
CA50-CA90	50–90% Cumulative Heat Release.
CA10-CA90	10–90% Cumulative Heat Release.
CAD	Crank Angle Degree.
CLD	Chemiluminescence Detector.
CO	Carbon Monoxide.
CO₂	Carbon Dioxide.

COV_{IMEP}	Coefficient of Variation of IMEP.
DAQ	Data Acquisition.
DF	Dual-Fuel.
DOC	Diesel Oxidation Catalyst.
D MDF	Diesel-Methanol Dual-Fuel.
ECR	Effective Compression Ratio.
ECU	Electronic Control Unit.
EGR	Exhaust Gas Recirculation.
EIVC	Early Intake Valve Closing.
FID	Flame Ionization Detector.
FSN	Filter Smoke Number.
GHG	Greenhouse Gas.
HCCI	Homogenous Charge Compression Ignition.
HRR	Heat Release Rate.
HC	Hydrocarbons.
HD	Heavy Duty.
IMEP	Indicated Mean Effective Pressure.
IVO	Intake Valve Opening.
IVC	Intake Valve Closing.
IS_{soot}	Net Indicated Specific Emissions of Soot.
IS_{NO_x}	Net Indicated Specific Emissions of NO _x .
ISCO	Net Indicated Specific Emissions of CO.
ISHC	Net Indicated Specific Emissions of Unburned HC.
LIVC	Late Intake Valve Closing.
LHV_{CO}	Lower Heating Value of Carbon Monoxide
LHV_{DF}	Actual Lower Heating Value in Dual-Fuel Mode.
LHV_{Diesel}	Lower Heating Value of Diesel.
LHV_{methanol}	Lower Heating Value of Methanol.
LTC	Low Temperature Combustion.
MFB	Mass Fraction Burned.
MF	Methanol Energy Fraction.
MK	Modulated Kinetics.
$\dot{m}_{methanol}$	Methanol Flow Rate.

\dot{m}_{diesel}	Diesel Flow Rate.
NDIR	Non-Dispersive Infrared Absorption.
NIE	Net Indicated Efficiency.
NO_x	Nitrogen Oxides.
P_{int}	Net Indicated Power.
PFI	Port Fuel Injector.
PM	Particulate Matter
P_{max}	Maximum In-cylinder gas pressure.
PCCI	Premixed Charge Compression Ignition.
PPCI	Partially Premixed Charge Compression Ignition.
PRR	Pressure Rise Rate.
RCCI	Reactivity Controlled Compression Ignition.
SCR	Selective Catalytic Reduction.
SOI	Start of Injection.
SOI_{main}	Main Injection Timing.
SOC	Start of Combustion.
TDC	Firing Top Dead Centre.
T_{int}	Intake air temperature.
UNIBUS	Uniform Bulky Combustion System.
V_{ivc_eff}	Effective Cylinder Volume.
V_{tdc}	Cylinder Volume at TDC.
VVA	Variable Valve Actuation.
θ	Crank Angle Degree.
γ	Ratio of Specific Heats.

659 **References**

- 660 1. Pachauri, R.K., “Climate Change 2014 Synthesis Report,” *Russ. Fed. Hoesung Lee*
661 *(Republic Korea) Scott B. Power N.H. Ravindranath* 167, 2014,
662 doi:10.1017/CBO9781107415324.
- 663 2. SMMT, “New Car CO 2 Report 2018,” 2018.
- 664 3. Gravel, R., “Freight Mobility and SuperTruck,” 2016.

- 665 4. Heywood J.B, "Internal Combustion Engine Fundamentals," ISBN 007028637X,
666 1988.
- 667 5. Barbosa, F.C., "Heavy Duty Emission Standards Assessment - An Engine and
668 Aftertreatment Technological Approach," *SAE Tech. Pap.*, 2016, doi:10.4271/2016-
669 36-0167.
- 670 6. Bendu, H. and Murugan, S., "Homogeneous charge compression ignition (HCCI)
671 combustion: Mixture preparation and control strategies in diesel engines," *Renew.*
672 *Sustain. Energy Rev.* 38:732–746, 2014, doi:10.1016/j.rser.2014.07.019.
- 673 7. Shi, L., Zhang, L., Deng, K., Lv, X., and Fang, J., "Experimental Research on Mixture
674 Distribution of Diesel Premixed Low-Temperature Combustion," 8, 2015,
675 doi:10.4271/2015-01-1839.
- 676 8. Musculus, M.P.B., Miles, P.C., and Pickett, L.M., "Conceptual models for partially
677 premixed low-temperature diesel combustion," Elsevier Ltd, ISBN 0360-1285, 2013,
678 doi:10.1016/j.pecs.2012.09.001.
- 679 9. Kimura, S., Aoki, O., Ogawa, H., Muranaka, S., and Enomoto, Y., "New Combustion
680 Concept for Ultra-Clean and High-Efficiency Small DI Diesel Engines," (724), 1999,
681 doi:10.4271/1999-01-3681.
- 682 10. Hasegawa, R. and Yanagihara, H., "HCCI Combustion in DI Diesel Engine," *SAE*
683 *Tech. Pap. Ser. 1*, 2010, doi:10.4271/2003-01-0745.
- 684 11. Reitz, R.D., "Directions in internal combustion engine research," *Combust. Flame*
685 160(1):1–8, 2013, doi:10.1016/j.combustflame.2012.11.002.
- 686 12. Benajes, J., Molina, S., García, A., Belarte, E., and Vanvolsem, M., "An investigation
687 on RCCI combustion in a heavy duty diesel engine using in-cylinder blending of diesel

- 688 and gasoline fuels,” *Appl. Therm. Eng.* 63(1):66–76, 2014,
689 doi:10.1016/j.applthermaleng.2013.10.052.
- 690 13. Paykani, A., Kakaee, A.H., Rahnama, P., and Reitz, R.D., “Progress and recent trends
691 in reactivity-controlled compression ignition engines,” *Int. J. Engine Res.* 17(5):481–
692 524, 2016, doi:10.1177/1468087415593013.
- 693 14. Wang, B., Yao, A., Yao, C., Chen, C., Lu, H., and Feng, J., “Experimental
694 investigation on methanol auto-ignition in a compression ignition engine under DMDF
695 mode,” *Fuel* 237(92):133–141, 2019, doi:10.1016/j.fuel.2018.09.154.
- 696 15. Verhelst, S., Turner, J.W., Sileghem, L., and Vancoillie, J., “Methanol as a fuel for
697 internal combustion engines,” *Prog. Energy Combust. Sci.* 70:43–88, 2019,
698 doi:10.1016/j.pecs.2018.10.001.
- 699 16. Varde, K.S., “Ignition Delay and Emissions Characteristics of a Methanol-Diesel
700 Fueled Engine at Low Charge Temperatures,” *SAE Tech. Pap. Ser. 1*, 2010,
701 doi:10.4271/920037.
- 702 17. Hanson, R.M., Kokjohn, S.L., Splitter, D.A., and Reitz, R.D., “An Experimental
703 Investigation of Fuel Reactivity Controlled PCCI Combustion in a Heavy-Duty
704 Engine,” *SAE Int. J. Engines* 3(1):2010-01–0864, 2010, doi:10.4271/2010-01-0864.
- 705 18. Kokjohn, S.L. and Reitz, R.D., “Characterization of Dual-Fuel PCCI Combustion in a
706 Light-Duty Engine Department of Mechanical Engineering University of Wisconsin -
707 Madison,” (July), 2009.
- 708 19. Kokjohn, S.L., Hanson, R.M., Splitter, D.A., and Reitz, R.D., “Fuel reactivity
709 controlled compression ignition (RCCI): A pathway to controlled high-efficiency clean

- 710 combustion,” *Int. J. Engine Res.* 12(3):209–226, 2011,
711 doi:10.1177/1468087411401548.
- 712 20. Pedrozo, V.B., May, I., Guan, W., and Zhao, H., “High efficiency ethanol-diesel dual-
713 fuel combustion: A comparison against conventional diesel combustion from low to
714 full engine load,” *Fuel* 230(February):440–451, 2018, doi:10.1016/j.fuel.2018.05.034.
- 715 21. Reitz, R.D. and Duraisamy, G., “Review of high efficiency and clean reactivity
716 controlled compression ignition (RCCI) combustion in internal combustion engines,”
717 *Prog. Energy Combust. Sci.* 46:12–71, 2015, doi:10.1016/j.pecs.2014.05.003.
- 718 22. Molina, S., García, A., Pastor, J.M., Belarte, E., and Balloul, I., “Operating range
719 extension of RCCI combustion concept from low to full load in a heavy-duty engine,”
720 *Appl. Energy* 143:211–227, 2015, doi:10.1016/j.apenergy.2015.01.035.
- 721 23. Asad, U. and Zheng, M., “Exhaust gas recirculation for advanced diesel combustion
722 cycles,” *Appl. Energy* 123:242–252, 2014, doi:10.1016/j.apenergy.2014.02.073.
- 723 24. Ladommatos, N., Abdelhalim, S.M., Zhao, H., and Hu, Z., “The Dilution , Chemical ,
724 and Thermal Effects of Exhaust Gas Recirculation on Diesel Engine Emissions - Part
725 4 : Effects of Carbon Dioxide and Water Vapour,” (412), 1997.
- 726 25. Hanson, R., Ickes, A., and Wallner, T., “Comparison of RCCI Operation with and
727 without EGR over the Full Operating Map of a Heavy-Duty Diesel Engine,” *SAE*
728 *Tech. Pap.* (x), 2016, doi:10.4271/2016-01-0794.
- 729 26. Wu, Y. and Reitz, R.D., “Effects of Exhaust Gas Recirculation and Boost Pressure on
730 Reactivity Controlled Compression Ignition Engine at High Load Operating
731 Conditions,” *J. Energy Resour. Technol.* 137(3):032210, 2015,
732 doi:10.1115/1.4029866.

- 733 27. Kavuri, C. and Kokjohn, S., “Investigating Air Handling Requirements of High Load
734 Low Speed Reactivity Controlled Compression Ignition (RCCI) Combustion,” 2016,
735 doi:10.4271/2016-01-0782.Copyright.
- 736 28. Duraisamy, G., Rangasamy, M., and Nagarajan, G., “Effect of EGR and Premixed
737 Mass Percentage on Cycle to Cycle Variation of Methanol/Diesel Dual Fuel RCCI
738 Combustion,” *SAE Tech. Pap. Ser. 1(x)*, 2019, doi:10.4271/2019-26-0090.
- 739 29. Benajes, J., Pastor, J. V., García, A., and Boronat, V., “A RCCI operational limits
740 assessment in a medium duty compression ignition engine using an adapted
741 compression ratio,” *Energy Convers. Manag.* 126:497–508, 2016,
742 doi:10.1016/j.enconman.2016.08.023.
- 743 30. Pedrozo, V.B. and Zhao, H., “Improvement in high load ethanol-diesel dual-fuel
744 combustion by Miller cycle and charge air cooling,” *Appl. Energy* 210(March
745 2017):138–151, 2018, doi:10.1016/j.apenergy.2017.10.092.
- 746 31. Kumar, C., Rana, K.B., and Tripathi, B., “Effect of diesel-methanol-nitromethane
747 blends combustion on VCR stationary CI engine performance and exhaust emissions,”
748 *Environ. Sci. Pollut. Res.* 6517–6531, 2019, doi:10.1007/s11356-018-04058-1.
- 749 32. Guan, W., Pedrozo, V., Zhao, H., Ban, Z., and Lin, T., “Exploring the NO_x Reduction
750 Potential of Miller Cycle and EGR on a HD Diesel Engine Operating at Full Load,”
751 *SAE Tech. Pap.* 2018-April:1–12, 2018, doi:10.4271/2018-01-0243.
- 752 33. Martins, M.E.S. and Lanzasova, T.D.M., “Full-load Miller cycle with ethanol and
753 EGR: Potential benefits and challenges,” *Appl. Therm. Eng.* 90:274–285, 2015,
754 doi:10.1016/j.applthermaleng.2015.06.086.

- 755 34. Zhao, J., “Research and application of over-expansion cycle (Atkinson and Miller)
756 engines ??? A review,” *Appl. Energy* 185:300–319, 2017,
757 doi:10.1016/j.apenergy.2016.10.063.
- 758 35. Benajes, J., Serrano, J.R., Molina, S., and Novella, R., “Potential of Atkinson cycle
759 combined with EGR for pollutant control in a HD diesel engine,” *Energy Convers.*
760 *Manag.* 50(1):174–183, 2009, doi:10.1016/j.enconman.2008.08.034.
- 761 36. Guan, W., Pedrozo, B., Zhao, H., Ban, Z., and Lin, T., “Variable valve actuation –
762 based combustion control strategies for efficiency improvement and emissions control
763 in a heavy-duty diesel engine,” *Int. J. Engine Res.*, 2019,
764 doi:10.1177/1468087419846031.
- 765 37. Ickes, A., Hanson, R., and Wallner, T., “Impact of Effective Compression Ratio on
766 Gasoline-Diesel Dual-Fuel Combustion in a Heavy-Duty Engine Using Variable Valve
767 Actuation,” *SAE Tech. Pap. Ser. 1*, 2015, doi:10.4271/2015-01-1796.
- 768 38. Pan, W., Yao, C., Han, G., Wei, H., and Wang, Q., “The impact of intake air
769 temperature on performance and exhaust emissions of a diesel methanol dual fuel
770 engine,” *Fuel* 162:101–110, 2015, doi:10.1016/j.fuel.2015.08.073.
- 771 39. Stricker, K., Kocher, L., Koeberlein, E., Alstine, D. Van, and Shaver, G.M.,
772 “Estimation of effective compression ratio for engines utilizing flexible intake valve
773 actuation,” *Proc. Inst. Mech. Eng. Part D J. Automob. Eng.* 226(8):1001–1015, 2012,
774 doi:10.1177/0954407012438024.
- 775 40. Pedrozo, V., “An experimental study of ethanol-diesel dual-fuel combustion for high
776 efficiency and clean heavy-duty engines,” PhD Thesis, Brunel University London,
777 2017.

- 778 41. Cheng, K.K. and W.K., “Speciated Engine-Out Organic Gas Emissions from a PFI-SI
779 Engine Operating on Ethanol/Gasoline Mixtures,” *SAE Int. J. Fuels Lubr.* 2,(No. 2
780 (2010),):91–101, 2010, doi:10.4271/2009-01-2673.
- 781 42. AVL., “AVL 415SE Smoke Meter,” *Prod. Guid. Graz, Austria*; 1–4, 2013.
- 782 43. Regulation No 49 – uniform provisions concerning the measures to be taken against
783 the emission of gaseous and particulate pollutants from compression-ignition engines
784 and positive ignition engines for use in vehicles. Off J Eur Union, 2013.
- 785 44. Zhao, H., “HCCI and CAI engines for the automotive industry,” ISBN
786 9781855737426, 2007.
- 787 45. Prashant, G.K., Lata, D.B., and Joshi, P.C., “Investigations on the effect of methanol
788 blend on the combustion parameters of dual fuel diesel engine,” *Appl. Therm. Eng.*
789 103:187–194, 2016, doi:10.1016/j.applthermaleng.2016.04.061.
- 790 46. Li, Y., Jia, M., Liu, Y., and Xie, M., “Numerical study on the combustion and
791 emission characteristics of a methanol/diesel reactivity controlled compression ignition
792 (RCCI) engine,” *Appl. Energy* 106(x):184–197, 2013,
793 doi:10.1016/j.apenergy.2013.01.058.
- 794 47. Authorities, A., “Acts Adopted By Bodies Created By International Agreements,” *Off.*
795 *J. Eur. Union* 7–9, 2013.
- 796 48. Pedrozo, V.B., May, I., Lanzasova, T.D.M., and Zhao, H., “Potential of internal EGR
797 and throttled operation for low load extension of ethanol–diesel dual-fuel reactivity
798 controlled compression ignition combustion on a heavy-duty engine,” *Fuel* 179:391–
799 405, 2016, doi:10.1016/j.fuel.2016.03.090.

Appendix A. Test cell measurement devices

Variable	Device	Manufacturer	Measurement range	Linearity/Accuracy
Speed	AG 150 Dynamometer	Froude Hofmann	0-8000 rpm	± 1 rpm
Torque	AG 150 Dynamometer	Froude Hofmann	0-500 Nm	$\pm 0.25\%$ of FS
Diesel flow rate (supply)	Proline promass 83A DN01	Endress+Hauser	0-20 kg/h	$\pm 0.10\%$ of reading
Diesel flow rate (return)	Proline promass 83A DN02	Endress+Hauser	0-100 kg/h	$\pm 0.10\%$ of reading
Intake air mass flow rate	Proline t-mass 65F	Endress+Hauser	0-910 kg/h	$\pm 1.5\%$ of reading
In-cylinder pressure	Piezoelectric pressure sensor Type 6125C	Kistler	0-300 bar	$\leq \pm 0.4\%$ of FS
Intake and exhaust pressures	Piezoresistive pressure sensor Type 4049A	Kistler	0-10 bar	$\leq \pm 0.5\%$ of FS
Oil pressure	Pressure transducer UNIK 5000	GE	0-10 bar	$< \pm 0.2\%$ FS
Temperature	Thermocouple K Type	RS	233-1473K	$\leq \pm 2.5$ K
Intake valve lift	S-DVRT-24 Displacement Sensor	LORD MicroStrain	0-24 mm	$\pm 1.0\%$ of reading using straight line
Smoke number	415SE	AVL	0-10 FSN	-
Fuel injector current signal	Current Probe PR30	LEM	0-20A	± 2 mA